Microstructured Polymer Optical Fiber Gratings and Sensors

52

Getinet Woyessa, Andrea Fasano, and Christos Markos

Contents

G. Woyessa (✉) · C. Markos
DTU Fotonik, Department of Photonics Engineering, Technical University of Denmark, Lyngby, Denmark
e-mail: gewoy@fotonik.dtu.dk; chmar@fotonik.dtu.dk

A. Fasano
DTU Mekanik, Department of Mechanical Engineering, Technical University of Denmark, Lyngby, Denmark
e-mail: andfas@kt.dtu.dk

G.-D. Peng (ed.), *Handbook of Optical Fibers*,
https://doi.org/10.1007/978-981-10-7087-7_2

Abstract

This chapter describes the realization of microstructured polymer optical fibers Bragg gratings (mPOFBGs) and their use in various sensing applications. Different grating inscription techniques based on different lasers used in recording grating in mPOF are presented. Grating inscription in mPOFs can be a challenging task compared to step index fibers because the microstructured cladding holes introduce scattering preventing the laser from reaching the core of the fiber easily. Inscription of gratings in mPOFs fabricated from different polymer materials such as Topas, Zeonex, Polycarbonate (PC) is discussed, and their optical and sensing performance is directly compared with the widely used poly(methylmethacrylate)(PMMA). The progress on fabrication of gratings in different types of mPOFs is presented in terms of grating inscription time, strength, and Bragg wavelengths. This chapter also describes the annealing process of mPOFs or mPOFBGs which is one of the curtail step in the development of stable mPOFBG sensors. The different annealing methods that have been applied by the research community are also presented. In addition, an overview on strain, humidity, temperature, pressure, and acceleration sensors developed from mPOFBGs is provided. A direct comparison in terms of their sensitivity, sensing range, and their performance in general is presented. Finally, the way to improve the development of stable mPOFBG sensors and widen their application areas is briefly discussed.

Microstructured Polymer Optical Fiber Bragg Gratings Inscription

Fiber Bragg gratings (FBGs) have been inscribed in microstructured polymer optical fibers (POFs) as in conventional step-index fibers based on different inscription techniques. The most common and used methods are the phase mask, point-by-point, as well as the interferometric method. Various types of lasers have been used for FBG inscription such as He-Cd laser, UV pulsed excimer laser, and ultrafast femtosecond lasers. The inscription of FBGs in microstructured polymer optical fibers (mPOFs) is not as straight forward as in step index POFs. The microstructured air hole pattern along the length of the fiber can significantly affect the writing process and the quality of the grating. Hence, the fiber should be aligned in such a way that the beam penetrates the highly scattering cladding and reaches the core easily, in order the inscription time to be reasonably short and the grating strength to be comparable with that of step index POFs. In this section, different types of FBG inscription methods in mPOFs and various types of laser used for inscription are reported as well as the effect of the microstructured cladding along the length of the fiber on the inscription process is discussed.

Interferometric Method

In this technique, UV laser beam from a single continuous wave (CW) laser source is split into two beams. This is commonly done by passing the beam through a 50:50 beam splitter. The two beams are then reflected by two mirrors and joined at angle θ after passing through two cylindrical lenses. The lenses are used to focus the UV laser beam and attain a high optical power density at the core of the mPOF. As the beams intersect, they produce periodic interference fringes, which, when they are focused onto the mPOF, effectively inscribe an FBG as shown in Fig. 1 (Meltz et al. 1989).

For a UV laser beam from a single source of wavelength λ and two beams incident on the fiber with an incidence angle θ with respect to the normal (Fig. 1), the period of the interference pattern formed as the two beams intersect, which corresponds to the period of the grating inscribed in the core of the mPOF fiber, is given by:

$$\Lambda = \frac{\lambda}{2 \sin(\theta)} \tag{1}$$

From Eq. 1, it can be seen that, using this writing technique, it is possible to inscribe an FBG with the intended periodicity (pitch) by simply adjusting the angle of incident of the two intersecting UV beams. Although this method gives this flexibility to control the period of the grating, it also has some drawbacks. The major disadvantage is that it requires a highly coherent UV beam laser source. Moreover, this coherence must be maintained throughout the exposure, otherwise a shift in the interference fringes may occur and thus the grating may undergo erosion. In addition, the beam alignment is time consuming and the mechanical stability is

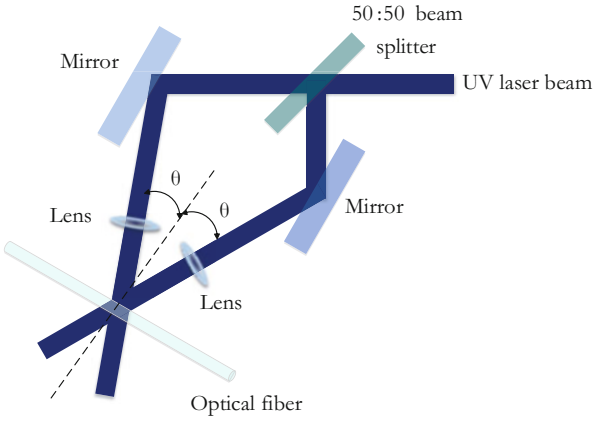

Fig. 1 FBG fabrication by transverse holographic technique

poor. For these reasons, the interferometric technique is not widely used in the FBG community even if it provides a great degree of flexibility.

Phase Mask Method

This inscription technique consists of a UV laser beam passing through the phase mask, which results the formation of a periodic interference pattern forming a grating in the mPOF. A phase mask is basically a plate of fused silica substrate which is transparent to the UV laser beam. One of the surfaces of the silica substrate is etched to create a surface relief structure which is periodic and has a square wave profile. In this technique, the phase mask is placed between the beam path and the mPOF as depicted in Fig. 2 (Hill et al. 1993). The UV light is directed to the phase mask, and after it passes through the periodic corrugations of the mask, the UV light splits into multiple diffracted beams in different directions, known as orders, defined as $m = 0, \pm 1, \pm 2, \pm 3$. These diffracted beams create a periodic interference pattern which, when exposed to an mPOF, photo-imprints a Bragg grating in the core of the fiber. The angle of diffraction, θ_m, can be calculated for each order based on the following diffraction Eq.:

$$m\lambda_{uv} = \Lambda_{pm} (\sin\theta_m + \sin\theta_i) \tag{2}$$

where, λ_{uv} is the wavelength of the inscription UV laser beam, Λ_{pm} is the period of the phase mask, and θ_i is the angle of incidence of the UV inscription beam to the top surface of the phase mask.

When the angle of incidence of the UV laser beam is normal to the top surface of the phase mask as shown in Fig. 2, which is the most commonly used configuration, Eq. 2 simplifies as follows:

$$m\lambda_{uv} = \Lambda_{pm} \sin\theta_m \tag{3}$$

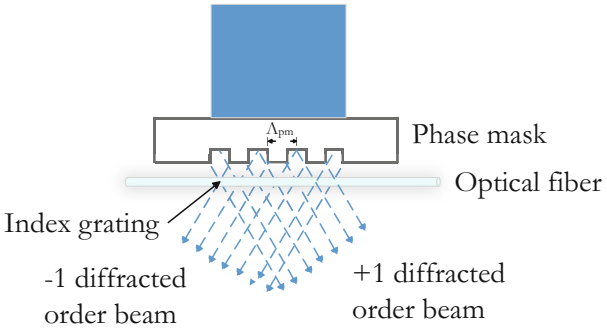

Fig. 2 UV laser beam passing through a phase mask and UV interference pattern generated from -1 and $+1$ diffraction orders of the phase mask

When the angle of incidence of the UV laser beam is perpendicular to the phase mask, the angles of diffraction are equal for both the positive and negative orders. For the majority of FBG fabrication processes, the diffracted light is limited to the orders −1, 0, and 1. Although most of the diffracted UV light beams are contained in −1, 0, and +1 diffracted orders, the most employed phase mask configuration normally suppresses the diffraction light beam contained in the zero order (Xiong et al. 1999). This can be achieved by controlling the depth of the corrugation in the phase mask. Thus, the period of the interference pattern formed by the −1 and +1 orders, hence the grating planes, Λ, is defined by both the UV laser beam wavelength, λ_{uv}, and the diffraction angle of the two beams.

$$\lambda_{uv} = \Lambda 2 \sin \theta_m \tag{4}$$

By using Eqs. 3 and 4, the period of the grating planes Λ is therefore one half of the period of the surface relief pattern of the mask Λ_{pm} as follows:

$$\begin{gathered} \lambda_{uv} = \Lambda 2 \sin \theta_m = \Lambda_m \sin \theta_m \\ \Lambda = \frac{\Lambda_{pm}}{2} \end{gathered} \tag{5}$$

From Eq. 5, it can be seen that the period of the grating is dependent only on the period of the phase mask and is independent of the wavelength of the UV laser beam irradiating the phase mask. Nevertheless, the corrugation depth required to suppress the diffracted beam of light contained in the zeroth order is a function of the wavelength of the UV laser beam (Williams 1997).

Figure 3 shows a complete schematic setup for microstructured polymer optical fiber Bragg grating (mPOFBG) inscription using the phase mask approach. As it can been seen, the main components of the setup are a UV laser, mirrors, cylindrical focusing lens, and phase mask. The UV laser light with a circular Gaussian beam profile is directed through a series of 4 mirrors and arrives at the focusing lens prior to the phase mask. The lens focus the beam through the phase mask down onto the fiber core. The phase mask is positioned parallel to the fiber surface as close as possible without actually touching it in order to protect the surface relief pattern of the mask from damage. The high intensity points of the pattern of the diffracted orders were projected into the mPOF core, resulting in a permanent periodic refractive index change within the mPOF core.

The most widely used UV laser for FBG inscription is He-Cd laser (IK5751I-G from Kimmon) operating at 325 nm. This laser has a circular Gaussian beam profile with a diameter of approximately 2 mm (Dobb et al. 2005; Johnson et al. 2010a; Stefani et al. 2011). Other types of lasers have been also used such as KrF excimer laser (Bragg Star *TM* Industrial-LN) operating at 248 nm (Oliveira et al. 2015). The KrF excimer laser has also Gaussian beam profile with a beam spot ∼6 mm in diameter and pulse duration of ∼15 ns. Femtosecond lasers have also been used for writing FBGs in mPOFs using phase mask technique. A 400 nm femtosecond laser pulse with a beam diameter of 6 mm has been used in the inscription of FBGs in doped poly (methylmethacrylate) (PMMA) mPOFs (Hu et al. 2017).

The phase mask approach has many distinct advantages over the other writing techniques. First, it allows the use of low-cost UV light source by lowering the requirement of the laser coherence, which is essentially required for transverse holographic technique. Second, it permits an easier arrangement of the fiber to be grated and also the stability requirements on the grating apparatus are reduced. This configuration set-up is mechanically stable and reliable, and FBGs are relatively easy to inscribe. Therefore, this method produces the most consistent and reproducible inscriptions, and hence it is the most common method of FBG writing in mPOFs. The main disadvantage of the phase mask technique is that to fabricate gratings with different pitches (i.e., different Bragg wavelengths), different phase masks are required, thereby increasing the production cost. It should be noted however that simple postprocessing approaches have been already reported which provide the ability to tune the grating to a certain degree. The most common one is by applying axial prestraining before inscription or postinscription annealing of the FBG. By using this method, it is possible to tune the grating by more than 250 nm (Yuan et al. 2012; Woyessa et al. 2016).

A typical interrogation system for the grating inscription in mPOF is also shown as a part of Fig. 3 which mainly consists of a broad band light source, a 3 dB coupler, and an optical spectrum analyzer (OSA). A broadband light source or a supercontinuum laser is used to couple the light into the core of the mPOF via the coupler and a silica fiber butt-coupled to the mPOF. Index matching oil is usually used in the gap between the silica fiber and the mPOF to minimize interference from the formed cavity and to reduce the reflection noise. The reflected signal from the

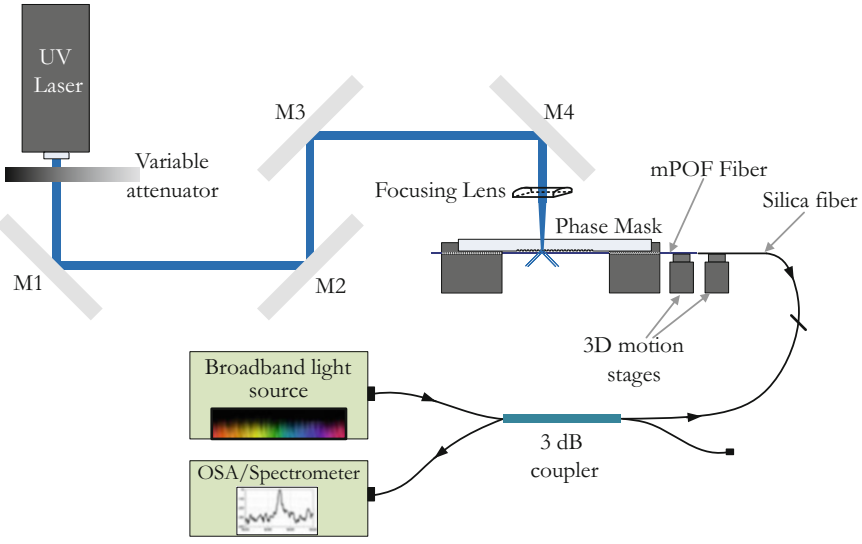

Fig. 3 One of the most commonly used FBG inscription and interrogation setups in mPOF using the phase mask technique

mPOFBG is coupled back through the 3 dB coupler, and finally it is collected from an optical spectrometer or the OSA.

Point-by-Point Method

In contrast to the inscriptions approaches described above, where the inscription process takes place in a single exposure to the laser beam, in the point-by-point approach, each grating plane in the mPOF core is photo-inscribed point by point by exposing the side of the optical fiber to a pulsed laser (Malo et al. 1993). Figure 4 shows the schematic representation of the FBG fabrication using the point-by-point method. In this method, the mPOF is first placed on a mechanical stage which enables the fiber to be translated along its length during the inscription process. Then a collimated UV or near infrared (near-IR) laser beam is focused on the core of the fiber from the side of the fiber to photo-imprint one grating plane at a time. The stage is then translated, hence the fiber, by a length which is the intended period of the grating, Λ, to write the next grating plane. The same procedure is repeated, until a periodic FBG is fabricated. The same technique has also been demonstrated with an ultrafast femtosecond pulsed laser (Martinez et al. 2004; Kalli et al. 2015).

A Ti:sapphire femtosecond laser system (Hurricane, Spectra-Physics) has been also used to inscribe gratings in PMMA mPOFs in the 1550 nm region (Stefani et al. 2012a). The output of the laser has 100 fs pulses with a central wavelength of 800 nm repetition rate of 1 kHz and average output power of 1 W. The significant advantage of the point-by-point grating technique is that it provides the choice of the length and pitch of the grating to be determined independently. This enables the location of the reflected wavelength to be controlled precisely and the use of expensive phase masks can also be avoided. Direct writing allows also the inscription of FBGs in nonphotosensitive materials. One of the main drawbacks of this fabrication approach is that it requires accurate alignment of the fiber core with the beam, while the continuous irradiation and translation process lead to extensive inscription durations compared, for example, to the previously described approaches.

The Effect of Microstructure in Grating Inscription

One of the most common challenges during FBG inscription in mPOFs is the scattering of the laser beam due to the presence of the cladding air-holes. This

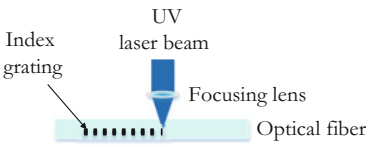

Fig. 4 FBG fabrication by point-by-point technique

usually prevents the laser beam from reaching the core of the mPOF. Thus, in order to achieve rapid inscription and high quality gratings in the mPOF, the orientation of the fiber has a crucial role in the process and it should be in such a way that the coupling of the laser beam to the core of the fiber is maximized. In a quest of finding the optimum fiber orientation, Marshall et al. preformed a thorough computational and experimental study to understand the effect of the microstructured air holes in the FBG inscription in microstructured optical fibers (Marshall et al. 2007). In their experiment, they focused a laser beam at 267 nm (3rd harmonic generated from 120 fs pulses at 800 nm, from a Spectra-Physics Hurricane) from the side on the core of the microstructured optical fiber. The laser beam was focused and coupled from the side to the core of the microstructured fiber, and then propagating to the tip of the fiber. From the tip of the fiber, the luminescence was measured and this process was repeated by rotating the fiber by one degree each time. It was found that the coupling of the laser beam to the core of the fiber was the strongest only for certain angles. Those are angles close to *X* but not exactly at *X* (see Fig. 5), the angular direction that offers direct access to the core for the laser light and hence the coupling to the core was the strongest. Another similar investigation on the effect of the microstructure on the grating inscription has been performed by T. Baghdasaryan et al. (2011). They used an ultrafast Ti:Sapphire laser at 800 nm by using different angular orientation and geometries of microstructured fibers. In their study, they also investigated the effect of the microstructured holes sizes and the hole to pitch ratio of the fiber. The results revealed that there is an orientation that gives the strongest coupling, which are angles close to *X*, and sufficiently small holes will result in a high quality grating, despite small air filling factor significantly reduces the strong confinement achievable in the microstructure optical fiber. Both of the above investigations were based on focusing the laser on the side of the fiber and measuring the photoluminescence at the tip of the fiber as the laser beam was guided through the core of the fiber.

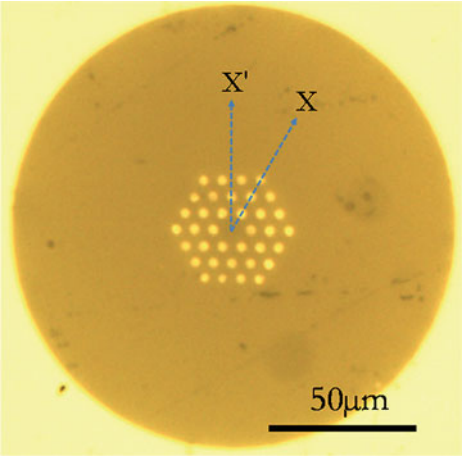

Fig. 5 Microscope image of mPOF with marked symmetry directions X' and X

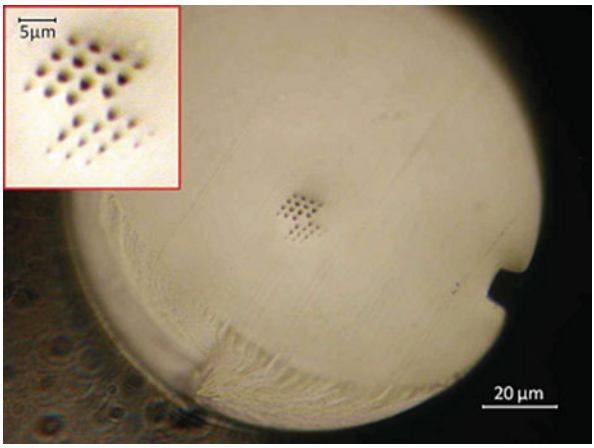

Fig. 6 Cross section of a mPOF designed for direct writing. Inset: zoom on the microstructure (Stefani et al. 2012a)

In 2015, Bundalo et al. experimentally demonstrated the above claims by inscribing a grating in mPOFs at various angles (Bundalo et al. 2015). They reached the same conclusion as Marshall et al. and T. Baghdasaryan et al. that certain angles can significantly assist in obtaining high quality gratings in mPOFs, which means fast inscription time and stronger gratings. They also showed that gratings could be obtained at almost any angle but the quality of the inscribed gratings was poor in terms of reflection strength and inscription time, if the fiber orientation was not in the proper range of angles, i.e., X'.

To minimize the effect of the microstructured air holes on the grating inscription and to access the core of the fiber with reduced difficulty, new fiber designs were proposed. For example, Stefani et al. designed and fabricated a PMMA mPOF for grating inscription using the point by point technique (Stefani et al. 2012a). The fiber was designed and fabricated to have the laser beam passing between the microstructure holes with minimum scattering before reaching the fiber core. To do so, six holes were removed from the three ring hexagonal microstructure, two from the outer ring and one from the second ring from both sides of the hexagonal configuration symmetrically as shown in Fig. 6. For the laser beam to pass the first ring of holes without encountering any interface, the pitch of the microstructure was designed to be bigger than the spot size of the laser beam. In addition, in order to facilitate the alignment of the microstructure, an alignment groove in the outer part of the fiber was also added.

Microstructured Polymer Optical Fiber Bragg Gratings

In this section, different mPOFs fabricated from different types of polymers are reported, and the progress on the fabrication of gratings in mPOFs in terms of inscription time, wavelength, and strength is presented. Currently existing mPOFs used for the grating fabrication are PMMA, Topas, Polycarbonate (PC), and Zeonex.

Fabrication of gratings in mPOF made from these polymer materials will be reported in the following sections.

PMMA mPOFBGs

The first FBG in mPOFs was inscribed by Dobb et al. in 2007 in the 1550 nm wavelength region (Dobb et al. 2005). The technique used for the inscription was the phase mask by using a 325 nm HeCd continuous wave UV laser with a power of 30 mW. The laser spot had a 1.8 mm diameter and it was expanded to 10 mm by cylindrical lens. The phase mask used for inscription had a uniform period of 1060.85 nm. Two types of PMMA mPOFs were used for the inscription: an endlessly single mode and a few modes fibers with hole to pitch ratio of 0.31 and 0.55, respectively. The FBGs inscribed in the single and few modes mPOFs have Bragg wavelength, FWHM, and reflection strength of 1569 nm, 0.5 nm and 5 dB, and 1570 nm, 1 nm and 7 dB, respectively. The length of the grating for both cases was 10 mm and the FBGs were saturated almost an hour after the exposure. Figure 7a and b shows the reflection spectrum and the growth dynamics of the fabricated gratings in a single and a few mode PMMA mPOF, respectively.

Some of the limitations of the FBG inscription process by Dobb et al. were the long writing time and the weak gratings. However, some years later (2014)

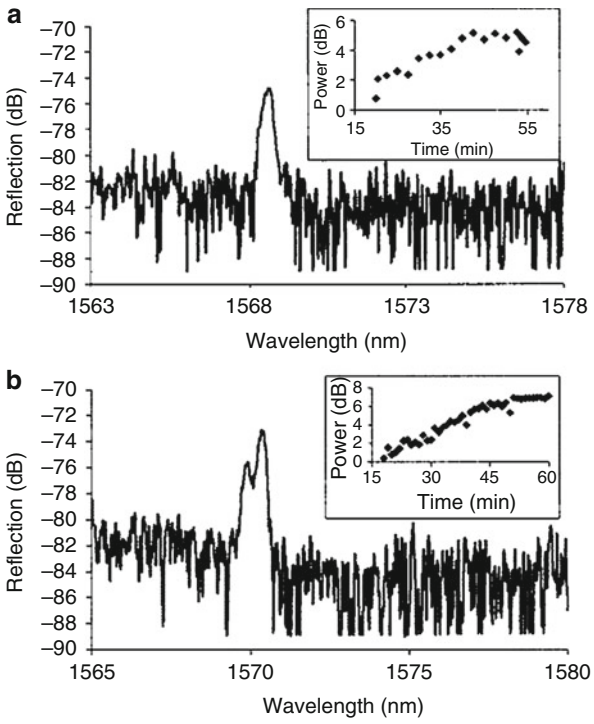

Fig. 7 (**a**) Reflection spectrum of an FBG fabricated in a single-mode PMMA mPOF. Inset: Growth of signal-to-noise ratio. (**b**) Reflection spectrum of an FBG fabricated in a few mode PMMA mPOF. Inset: Growth of signal-to-noise ratio (Dobb et al. 2005)

Bundalo et al. reported FBG inscription in PMMA mPOFs with a writing time 10 times shorter than it was previously reported (Bundalo et al. 2014). The setup used by Bundalo et al. was also a standard phase mask writing technique except that in this case the HeCd laser beam was not expanded. It was demonstrated that there was a strong correlation between laser power and the grating inscription time revealing that a high intensity of laser power in the core was required in order to obtain a fast writing time. The fiber used was an endlessly single mode 3 rings PMMA mPOF with a hole to pitch ratio of 0.26. The phase mask used in their experiments had a uniform pitch of 424.84 nm which is suitable for writing FBGs in the 650 nm wavelength region. The fastest inscription time achieved was less than 7 min with full laser power of 30 mW. The grating had the following characteristics: reflection strength, FWHM, and Bragg wavelength of 26 dB, 0.4 nm, and 632.6 nm, respectively. The length of the grating was 2 mm and it was shown that there was no dependence between the laser power and the grating strength. However, low laser inscription powers resulted in longer writing times. By using 72% of the full laser power, an FBG of the same strength but with longer inscription time, around 18 min, was obtained. Table 1 summarizes the comparison of the growth rates and the quality of the gratings for 6 inscription trials made in PMMA mPOFs. Bundalo et al. claimed that the most important factors leading to these results were the removal of the beam expansion lens and the careful alignment of the laser beam in the core of the mPOF. The laser power reaching the fiber without using the beam expanding lens was 7–8 times more intense than with the beam expansion lens.

A year later Oliveira et al. reported the inscription of FBGs in a PMMA mPOF in less than 30 s using the phase mask method (Oliveira et al. 2015). Despite they used the phase mask writing technique, the laser for inscription was not the same as the one used by Dobb et al. and Bundalo et al.; they rather used a KrF excimer laser (Bragg Star *TM* Industrial-LN) at 248 nm wavelength. They claimed that the key factors leading to such reduced writing time were the use of low number of pulses, low repetition rate, and low fluence. They revealed that by using energy density below the threshold for the PMMA ablation, it is possible to avoid the damage of the surface of the polymer fiber and increase the refractive index change in the core of the fiber. The fiber used in their experiments was a few mode 6-ring PMMA mPOF with a hole to pitch ratio of 0.52. The phase mask had a uniform

Table 1 Comparison of growth rates, grating saturation time, FWHM, and grating strength for six grating inscription attempts in PMMA mPOFs

FBG	Grating growth rate (dB/min)	Grating saturation time (mm:ss)	Grating FWHM (nm)	Grating strength (dB)
1	7.9	06:50	0.4	26
2	3.99	08:50	0.35	24
3	3.7	07:10	0.3	19
4	3.18	17:50	0.4	26
5	2.47	15:00	0.4	21
6	2.1	15:50	0.425	15

period of 1023 nm and the laser beam was not expanded. The laser beam passed through a slit of 4.5 mm width and was shaped before reaching the phase mask. The Bragg wavelength, the reflection strength, and 3 dB bandwidth of the grating were 1515 nm, 20 dB, and 0.16 nm, respectively. The length of the grating was 4.5 mm and it was inscribed with 1 Hz repetition rate, 33 mJ/cm^2 fluence, and 20 pulses. Figure 8 shows the growth dynamics of the grating during the grating inscription. This inscription time is the shortest writing time in POFs till now by using a UV laser. One of the advantages of having a fast inscription time is that the constraint related to the stability of the mechanical setup during the inscription process can be minimized.

The above-mentioned FBG inscriptions in PMMA mPOFs were done with a UV laser. However, PMMA mPOFs have also been inscribed with femtosecond laser by using the point by point inscription method. Stefani et al. reported the fabrication of FBGs in PMMA mPOF with 800 nm Ti:sapphire femtosecond laser system (Hurricane, Spectra-Physics) using direct-writing techniques (Stefani et al. 2012a). To avoid scattering before the laser reaching the core and facilitate the inscription process, they used a different fiber design which is shown in Fig. 6 in the previous section. The fiber had air filling factor in between 0.29 and 0.43. Despite this fiber design facilitated the inscription process, it is clear that it had higher confinement loss and high birefringence compared to the standard three ring fiber, thus reducing the quality of the grating as shown in Fig. 9. The grating was a fourth-order Bragg grating with a pitch of around 2 μm and Bragg wavelength at 1518.67 nm. The grating was 5 mm long and it took 2.5 s writing time for this length. This writing time is even much shorter than the one achieved with KrF laser for almost the same grating length.

Bragg gratings in PMMA mPOFs have also been fabricated at different wavelengths using different phase masks. Johnson et al. fabricated an FBG in a multimode (MM) PMMA mPOF with a core dimeter of 50 μm at 827 nm (Johnson et al. 2010a). The inscription system was a standard phase mask method and the

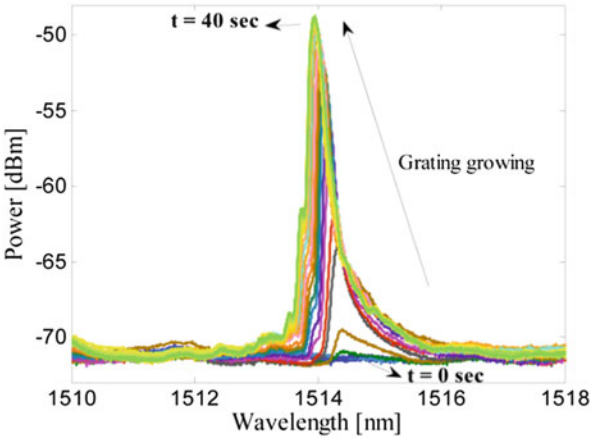

Fig. 8 Growth dynamic of the 4.5 mm grating in a few mode PMMA mPOF during writing using a KrF excimer laser (Oliveira et al. 2015)

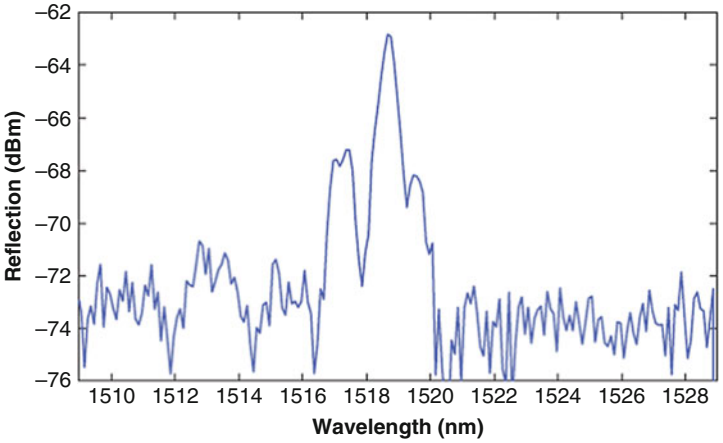

Fig. 9 Measured reflection spectrum of the fourth-order grating inscribed with the point by point method (Stefani et al. 2012a)

inscription laser was a 325 nm HeCd UV laser. The phase mask had a uniform period of 557.2 nm. The grating had 1.8 mm length and 7.5 dB strength in the reflection with FWHM of 2.45 nm. This grating was inscribed in 2 h. Stefani et al. inscribed FBGs in a few mode PMMA mPOFs at 850 nm (Stefani et al. 2011). The inscription system used was similar to the one used by Johnson et al. with the only difference that laser beam was expanded to 10 mm. The phase mask had a uniform period of 572.4 nm. The grating was 10 mm long and 10 dB strength in reflection with FWHM of 0.29 nm. The writing time was ∼185 min.

Most of the FBGs inscribed in mPOFs are single gratings which are the result of the ±1 diffraction orders of the phase mask. Barabach et al. fabricated multiple FBGs in PMMA mPOFs using a phase mask with several diffraction orders (Statkiewicz-Barabach et al. 2013). They used a HeCd UV laser and a standard phase mask inscription technique. The fiber used was a standard three ring mPOF with hole to pitch ratio of 0.48, and it was fabricated from a commercial available PMMA rod. The phase mask used had a higher diffraction order ±2 and ±3 with large efficiency in addition to the ±1 diffraction order. The phase mask had a period of 1.052 μm, and it gave a fundamental Bragg peak at $\lambda_B = 1555$ nm and higher order peaks at $\lambda_B/2$ and 2/3 λ_B. The detailed numerical simulation performed by Barabach et al. showed that the formation of the Bragg peaks at $\lambda_B/2$ and 2/3 λ_B could be attributed either to the first order reflection from the gratings with a periodicity of $\Lambda/4$ and $\Lambda/3$ or to the second and third order reflection from the grating of period Λ. The inscription of these multiple gratings took around 40 min. Figure 10 shows the reflection spectrum of the multiple gratings inscribed in PMMA mPOF using a single-phase mask with a single exposure.

All the PMMA mPOFBGs discussed above are inscribed in an undoped fiber. Sáez-Rodríguez et al. doped a core of PMMA mPOF with BDK to increase the

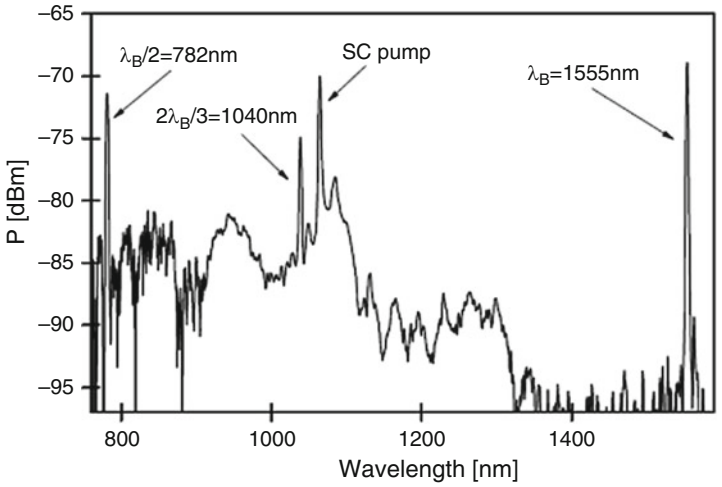

Fig. 10 Reflection spectrum recorded during the fabrication process (at the 28th min of exposure) of multiple Bragg gratings in PMMA mPOF (Statkiewicz-Barabach et al. 2013)

photosensitivity of the fiber and hence obtain a shorter writing time and a higher index change compared to the undoped one (Sáez-Rodríguez et al. 2013). The fiber fabricated had a hole to pitch ratio of 0.47. To inscribe the grating in the BDK doped fiber, they used a HeCd UV laser and a standard phase mask inscription technique. The laser beam had a diameter of 1.2 mm and the final grating length was 3.8 mm. However, to increase the length of the grating, the inscription was carried out using a mirror mounted on a motorized translation stage to scan a beam of 1.2 mm diameter focused with a cylindrical lens along the longitudinal axis of the fiber through a phase mask of pitch 557.5 nm, rather than expanding the beam. The grating was 23 dB strong in transmission with a 10 dB bandwidth of 0.3 nm. The corresponding inscription time was only 13 min. The microscope image of the end facet of the doped fiber used for the grating inscription and the grating growth dynamics is shown in Fig. 11a and b, respectively. Hu et al. also inscribed FBGs in BDK doped PMMA mPOF (Hu et al. 2017) using 400 nm femtosecond laser pulses with a beam diameter of 6 mm and a 1060 nm period uniform phase mask for the inscription. The fiber was fabricated purely from PMMA except that the core was BDK doped. The filling factor of the microstructure region was 0.4. Hu et al. achieved a grating with 40% reflectivity in 20 s. The microscope image of the end facet of the doped fiber used for the grating inscription and the grating growth dynamics is shown in Fig. 12a and b, respectively.

Topas mPOFBGs

In addition to PMMA mPOFs, FBGs have also been inscribed in mPOF made of different polymer materials such as Topas, PC, and Zeonex. The motivation behind

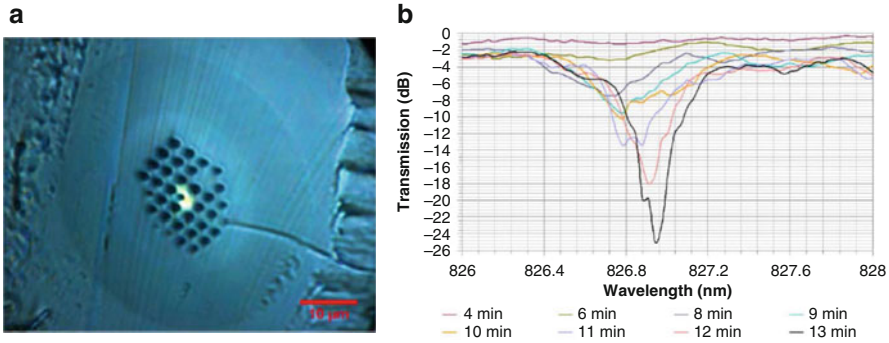

Fig. 11 (**a**) Microscope image of BDK doped PMMA mPOF. (**b**) The growth dynamics of the grating in transmission for the first 13 min (Sáez-Rodríguez et al. 2013)

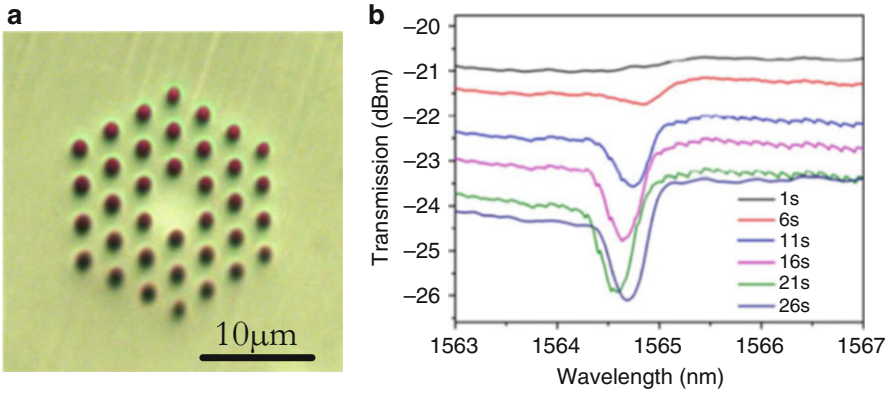

Fig. 12 (**a**) Microscope image of BDK doped PMMA mPOF. (**b**) Evolution of the transmitted amplitude spectrum during the photo-inscription process (Hu et al. 2017)

investigating new polymers for FBG sensors is due to the fact that different polymers have their own unique properties which are suitable for different FBG-based sensing applications. In this section, the fabrication of gratings in two different grades of Topas polymer is described. Topas belongs to the class of cyclic olefin copolymers (COCs), which is a class of optical thermoplastics that have a very low moisture uptake, chemical inertness to acids and bases, and many polar solvents (Topas COC 2014).

The first Topas mPOF was fabricated from Topas grade 8007F-04 (Johnson et al. 2011). This grade of Topas has a glass transition temperature of 78 °C and water absorption (saturation) at 23 °C less than 0.01% (Data Sheet Topas 8007F-04 2015). The fabricated fiber had 2 rings of holes with hole to pitch ratio of 0.44. A grating was also inscribed with a standard phase mask method and 30 mW 325 nm HeCd UV laser. The phase mask had a uniform pitch of 1034.2 nm. It required 45 min for the grating to reach a saturation level. The 1.8 mm grating had a Bragg wavelength of 1567.9 nm with a FWHM of 0.75 nm and 18 dB strength in the reflection.

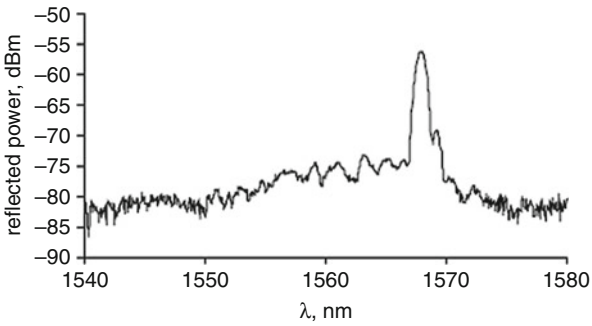

Fig. 13 Reflection spectrum of an FBG inscribed in Topas grade 8007F-04 mPOF (Johnson et al. 2011)

Figure 13 shows the reflection spectrum and the growth dynamics of the first grating inscribed in Topas-based mPOF.

Yuan et al. demonstrated also the inscription of an FBG in the same grade of Topas but in 850 nm spectral region, using a phase mask of a uniform period of 572.4 nm (Yuan et al. 2011). The main advantage of inscribing FBGs in the 850 nm region is that the loss of the fiber is very low compared to 1550 nm region which enables the use of longer fibers. The grating was inscribed with the same laser and technique as used by Johnson et al. (2011). The only difference is that here the UV laser beam was expanded from 1.2 mm to 12 mm. The resulted grating had a Bragg wavelength of 870 nm with FWHM less than 0.3 nm and reflection strength of 12 dB. The writing time was around 300 min.

Markos et al. reported the fabrication of FBGs in a different grade of Topas, commercially known as grade 5013S-04 (Markos et al. 2013). This grade of Topas had a glass transition of temperature (T_g) of 134 °C, 56 °C higher than Topas grade 8007F-04 and 25 °C higher than that of PMMA (Data Sheet Topas 5013S-04 2015). The water absorption capability is the same as Topas grade 8007F-04. But the main advantage of this grade of Topas is that it can be used to sense strain at high temperature as the T_g is relatively very high. The fabricated fiber had three rings of holes with hole to pitch ratio of 0.4, which is an endlessly single mode. The grating was fabricated with the same method and phase mask as used by Yuan et al. (Yuan et al. 2011). The limitation of this grade of Topas polymer is that it is difficult to draw fibers as it has a high flowability (Woyessa et al. 2017a).

Polycarbonate mPOFBGs

The first solid core polycarbonate (PC) mPOF was recently reported by Fasano et al. (2016). The motivation behind the fabrication of optical fibers from PC polymer lies in its T_g and the very good mechanical properties of the material. The T_g of PC is 145 °C and it is the highest among the currently existing mPOFs. Thus, FBGs fabricated in PC mPOFs can be used to sense temperature levels that PMMA and Topas mPOFBGs cannot reach. The other important advantage of PC is that it

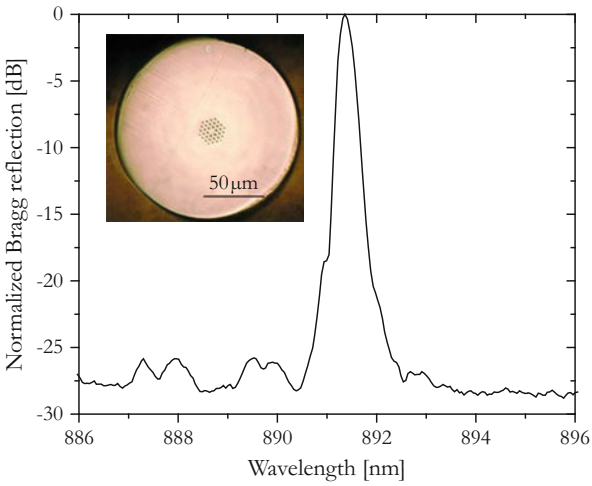

Fig. 14 PC mPOFBG reflection spectrum. Inset: Optical microscope image of the end facet of PC mPOF (Fasano et al. 2016)

usually yields and breaks at elevated values of strain (Optical properties of Makrolon and Apec 2014), and it is highly flexible in bending. The PC mPOF fabricated and characterized by Fasano et al. had a hole to pitch ratio of 0.4 ensuring thus endlessly single mode operation. The grating was inscribed with the phase mask technique and a 50 mW HeCd UV laser. For the grating inscription, the laser power was attenuated down to 4 mW which was found to be the suitable power for writing an FBG in the PC mPOF. The phase mask had a 572.4 nm uniform period. The grating had a Bragg wavelength of 892.4 nm with a FWHM of 0.46 nm and reflection peak of 25 dB. The required writing time was only 6 min by using only 4 mW power. Figure 14 shows the reflection of FBGs inscribed in the PC mPOF.

Zeonex 480R mPOFBGs

The polymer Zeonex 480R belongs to the class of cyclo-olefin polymers; in particular it is an amorphous homopolymer of norbornene. Zeonex 480R shares some of properties with Topas 5013S-04, such as low water absorption, high temperature resistance, and good chemical inertness to bases and acids (Khanarian and Celanese 2001). The T_g of Zeonex 480R is 138 °C (Technical data, Zeonex, Cyclo Olifen Polymer (COC) 2017). However, there are some fundamental differences regarding the chemical structure of Zeonex and Topas which make Zeonex better than Topas for the manufacturing of mPOFs. The main difference in their chemical structure is that Topas is not a homopolymer but an amorphous ethylene-norbornene copolymer with a high percentage of norbornene (Roy et al. 2012). Some of the unique advantages of Zeonex 480R are: its lower flowability compared to Topas 5013S-04, as well as its better transmittance, higher sensitivity to temperature, and better mechanical stability at high temperatures. Furthermore, Zeonex has very good compatibility with PMMA for co-drawing applications,

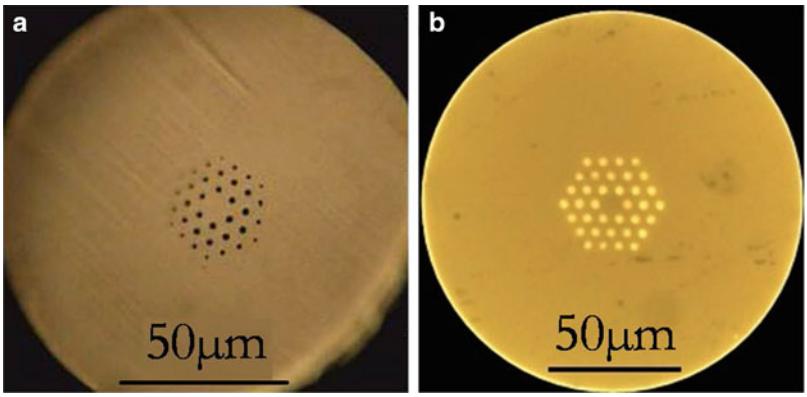

Fig. 15 Optical microscope image of the end facet of (**a**) Topas 5013S-04 (Markos et al. 2013). (**b**) Zeonex 480R mPOFs (Woyessa et al. 2017a)

low birefringence, and superior moldability (Technical data, Zeonex, Cyclo Olifen Polymer (COC) 2017; Leon-Saval et al. 2012). The first endlessly single mode Zeonex mPOF for Bragg grating sensing was fabricated and characterized by Woyessa et al. in 2017 (Woyessa et al. 2017a). It was fabricated from Zeonex grade 480R and the fiber had a hole to pitch ratio of 0.4. Woyessa et al. observed that during the drawing process of microstructured fibers, Zeonex 480R showed a superior drawability over Topas 5013S-04. This was due to the fact that the physical properties of Zeonex are well suitable for high quality fiber drawing. This fact is a direct consequence of Zeonex greater molecular weight. The weight-average molecular weight (M_w) of Zeonex 480R is six times larger than that of Topas 5013 (Roy et al. 2012; Torres et al. 2015), although their glass transition temperatures are similar, being 138 °C and 134 °C, respectively. For thermoplastic materials, the melt flow index defined as the flowability in general decreases with increasing M_w (Bremner et al. 1990). Therefore, Zeonex 480R preforms tend to flow slower than Topas 5013 under similar fiber drawing conditions, thereby ensuring highly controllable and stable fiber draw process. The other important advantage of having a lower melt flow rate is that it can allow getting a wide range of drawing temperature and stress. Therefore, the final mechanical properties of Zeonex 480R mPOFs can be tuned relatively more easily compared to that of Topas 5013S-04. As a result, Zeonex 480R allows a greater number of degrees of freedom in fiber design as the desired microstructures can be transferred to the final fiber more efficiently. For example, the cladding holes are uniform and symmetrical with minor distortions in their shape compared to Topas 5013 mPOFs (see Fig. 15). Due to the better stability of the drawing process, fluctuations in the fiber diameter are also reduced. Nevertheless, it should be noted that either too high or too low values of M_w can make the fiber drawing very challenging or even unfeasible. The M_w of Zeonex 480R is sufficiently low to avoid this potential problem.

A Bragg grating inscribed in the low loss spectral region of the Zeonex mPOF with the phase mask technique and a 50 mW HeCd UV laser has been also reported. For the grating inscription, the laser power was attenuated down to 5.5 mW which was suitable power for writing FBGs in Zeonex mPOFs. The phase mask had a uniform of 572.4 nm. The grating length was 2 mm and has a Bragg wavelength of 865.24 nm with a FWHM of 0.522 nm and reflection peak of 30 dB. The writing time was only 5 min by using a power of 5.5 mW.

The aforementioned polymers were shown to be photosensitive under 325 nm HeCd UV laser irradiation which enabled successful fabrication of gratings in the mPOFs. Materials alternative to PMMA, which is the standard material for polymeric Bragg gratings, have been developed to meet different needs, e.g., for insensitivity to humidity (Topas 8007 and 5013, Zeonex 480R), high thermal resistance (PC, but also Zeonex 480R and Topas 5013), and ease of fabrication (Zeonex 480R) (Johnson et al. 2011; Yuan et al. 2011; Markos et al. 2013; Woyessa et al. 2017a; Fasano et al. 2016).

Annealing of mPOFBGs

During the fabrication of an mPOF, the fiber is drawn under certain levels of drawing tension. This drawing stress aligns the molecular chain of the polymer along the fiber axis, thus leaving some residual stress. The alignment level depends on the amount of drawing tension applied during the fabrication process. When mPOFs are heated at a temperature close to their T_g, the polymer chains starts to relax from their original orientation formed during drawing. The amount of temperature that causes this process highly depends on the amount of stress applied when the fiber is fabricated, the thermal history of the preform from which the fiber is made, the amount of relative humidity (RH) in the vicinity of the fiber where the fiber is heating up, and the extent of UV exposure experienced by the fiber (Carroll et al. 2007; Ishigure et al. 2004; Shafee 1996). As the fiber is heated up, it shrinks and there will be a decrease in the length of the fiber and an increase in its diameter. This process is called annealing and leads to an irreversible change in the fiber dimensions. As mPOFBGs are annealed, the period of the Bragg grating decreases as the fiber shrinks and thus the grating experiences a permanent blue shift. The annealing of mPOFs either before or after inscription of a grating is a vital step in the development of stable mPOFBG sensor system. In this section, different methods of annealing of mPOFs and what advantages they can offer in the realm of mPOFBG sensors are discussed.

Temperature Assisted Annealing

In 2010 Johnson et al. showed for the first time the effect of thermal annealing on PMMA mPOFBGs (Johnson et al. 2010b). They first inscribed an FBG in MM PMMA mPOF using a phase mask with a period of 1057.2 nm producing a

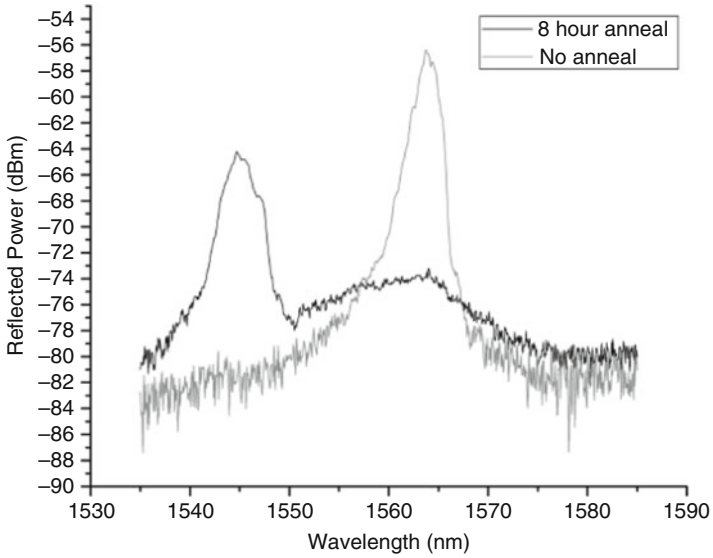

Fig. 16 Reflection spectrum of a MM PMMA mPOF before and after thermal annealing in a conventional oven at 80 °C for 8 h (Johnson et al. 2010b)

Bragg wavelength of 1562 nm. The grating was then annealed in a conventional oven at a constant temperature of 80 °C for 8 h. The thermal annealing induced a permanent blue shift of the reflected wavelength of ∼18 nm. Figure 16 shows the reflection spectrum of the grating before and after the annealing. The permanent wavelength shift was probably induced by a permanent shrinkage of the MM mPOF, which resulted in a decrease of the grating pitch. Thus, thermal annealing offers the possibility of tuning of FBGs within a certain range. This feature of thermal annealing of mPOFBG was further used to develop the first wavelength division multiplexed (WDM) FBG sensor by using a single-phase mask.

Carroll et al. demonstrated how thermal annealing of PMMA mPOFBGs or annealing the fiber before the grating inscription affects the thermal response of the grating (Carroll et al. 2007). They showed that PMMA mPOFBGs that were not annealed had a linear temperature operational response only up to 50–55 °C. They demonstrated the maximum operating temperature range of the grating, by heating up the grating in cycles up to certain temperature levels. The grating was heated by heating element in three different cycles, up to 77 °C, 86 °C, and 92 °C for the first, second, and third cycle, respectively. In the first cycle, the reflection spectrum linearly shifted to the blue from 23 °C to 55 °C. However, after this temperature range, the grating was shift to the blue very rapidly up to 77 °C and the shift was nonlinear. They found out that the thermal-induced blue-shift was permanent when they measured the spectrum again at room temperature and the shift was −8.4 nm. In the second cycle, the linear region was up to 76 °C, which was very close to the maximum temperature applied to the grating during the first cycle. After this

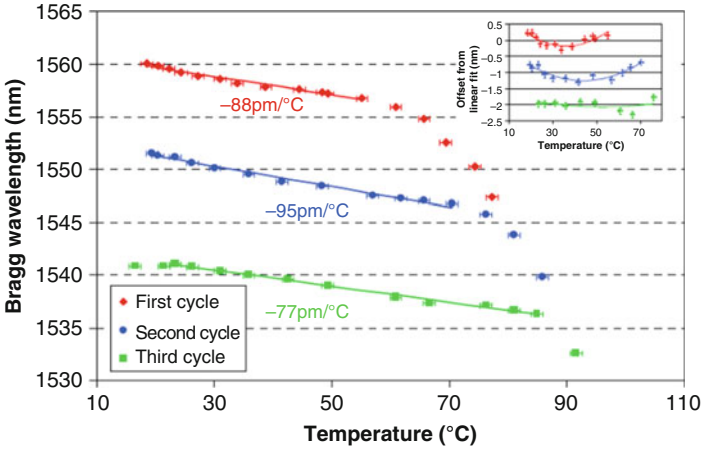

Fig. 17 Bragg wavelength shift with temperature for three consecutive heating cycles. Inset: Deviation from linear response for each cycle (data from successive cycles are offset by −1 nm for clarity) (Carroll et al. 2007)

temperature, the grating shifted to the blue again very rapidly up to 86 °C. When the temperature was decreased back to 23 °C from 86 °C, the grating shifted again permanently by −10.1 nm. In the third cycle, the grating operated linearly up to 86 °C. After this temperature, the observed rate of Bragg wavelength shift was fast up to 92 °C, as seen for the previous cycles. This process can be seen in Fig. 17. This investigation showed that thermal annealing is vital and essential step in order to achieve a linear and wide range of thermal response of a grating.

Temperature- and Humidity-Assisted Annealing

Annealing of mPOFBGs performed by both Johnson et al. and Carroll et al. was using conventional oven or simple heating elements. In this type of heating devices, humidity is not controlled. However, early investigations showed that humidity has a huge influence in the T_g of PMMA such that PMMA materials exposed to wet environment have a lower T_g than the one exposed to dry environment (Smith and Schmitz 1988). Woyessa et al. implemented a detailed experimental investigation on the combined effect of humidity and temperature on mPOFBGs (Woyessa et al. 2016). They reported that the RH has a great impact on the annealing of mPOFBGs. In particular they revealed that annealing mPOFBGs at high humidity and temperature resulted in an improved performance of mPOFBGs in terms of stability and sensitivity to humidity. In their investigation, an FBG was fabricated in an endlessly single mode PMMA mPOFs by using a phase mask with period 572.4 nm producing a Bragg wavelength at 850 nm. The annealing was done in a climate chamber which provides the ability to control

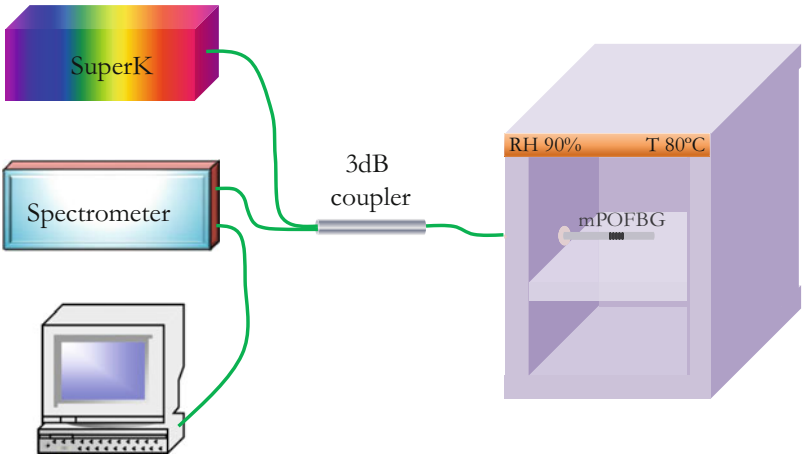

Fig. 18 Experimental setup used for temperature and humidity controlled annealing of PMMA mPOFBGs (Woyessa et al. 2016)

both temperature and humidity simultaneously. The experimental setup used for the annealing investigation is shown in the following Fig. 18.

In their experiments, firstly the climate chamber was set to a temperature and RH of 25 °C and 50%, respectively, which defined as the ambient conditions. Then after 2 h of ambient conditions, the RH of the chamber was decreased to 10% without changing the temperature. Three hours after 10% RH and 25 °C environmental conditions in the climate chamber, the temperature was ramped up to 80 °C at a fixed 10% RH. As the temperature was increasing to 80 °C, the mPOFBG was blue shifting rapidly. After 20 h the grating started to get stabilized. When the rate of the blue shift becomes 0.3 nm per hour (defined as the mPOFBG equilibrium condition), the RH of the chamber was increased by 20%, thus to 30%, yet at a fixed temperature of 80 °C. The grating was blue shifted by ∼66.33 nm before the RH was increased by 20%. As the RH increased to 30%, the grating again started to blue shift rapidly. After 23 h the rate of the shift reached to 0.3 nm per hour and the chamber RH was increased to 50%, then to 70% and finally to 90%, for each case when the equilibrium condition was reached. This process is depicted in Fig. 19, whereas the amount of blue shift and the time taken for each RH level are summarized in Table 2.

As it can be seen from Fig. 19 and Table 2, as the temperature was ramped up from 25 °C to 80 °C there was a fast blue-shift of the reflected wavelength as initially the fiber was releasing the frozen-in stress induced during the fabrication process very fast. However, 20 h later, the rate of shift became low and again increased as the RH was increased. At higher levels of RH such as 70% and 90%, not only the rate of the blue-shift was faster but also the amount of the shift was larger. This phenomenon is due the fact that PMMA has a high water absorption

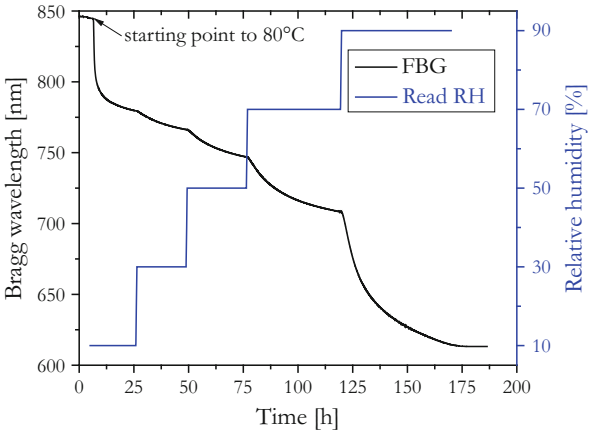

Fig. 19 Resonance wavelength of PMMA mPOFBGs during annealing at 80 °C and up to a RH of 90% starting from 10% and by 20% increment

Table 2 Summary of the amount of blue shift of the Bragg wavelength and the time taken during annealing of PMMA mPOFBGs at 80 °C and up to a RH of 90% starting from 10% and by 20% increment

RH (%)	Amount of blue shift (nm)	Time taken (hh:mm)
10	66.33	20:00
30	13.20	23:00
50	19.29	27:30
70	38.71	43:00
90	93.83	50:36

capability and water acts as a plasticizer for PMMA and hence decreases its T_g (Smith and Schmitz 1988). Thus, this investigation revealed for the first time that it is possible to tune the location of the Bragg wavelength in POFBGs by a relatively big amount by assisting the thermal annealing with humidity. The specific response of these PMMA-based mPOFBGs to humidity will be described in detail in section "Humidity Sensors." One of the potential advantages of humidity assisted thermal annealing is that it allows production of gratings at short wavelengths (large blue-shifts) in the visible range where POFs have lower loss but where the phase mask technique poses limitations in terms of efficiency and cost.

Chemical-Assisted Annealing at Room Temperature

The mPOF annealing methods discussed so far are activated thermally. It is the temperature that allows for the polymer chains to relax from their frozen in stresses. Furthermore, it has been shown that humidity facilitates the process as it lower the T_g of PMMA mPOFs. As the goal of annealing mPOFs is relaxing the frozen polymer chains, the question that may rise is, are there any other possible techniques that help the polymer chains to relax without increasing the temperature from

the room condition? Fasano et al. interestingly demonstrated for the first time the possibility of annealing of mPOFBGs in methanol-water solutions at room temperature. This was based on early studies by Williams et al., which showed the effect of the presence of methanol on the T_g of PMMA (Williams et al. 1986). This investigation revealed that for methanol-equilibrated PMMA systems the T_g is ranging from 20 °C to 30 °C depending on the weight-average molecular weight (M_w). Fasano et al. investigated this effect systematically using gratings inscribed in PMMA mPOF (Fasano et al. 2017) from the same fiber draw and CHROMASOLV methanol (for HPLC, $\geq$ 99.9% by weight, Sigma-Aldrich)/Milli-Q water concentrations, 50:50%, 60:40%, and 70:30% v/v, where water was used as a diluent for methanol. For each solution, two different grating were prepared. The gratings were immersed in the solution and their Bragg wavelength was monitored throughout the experiments. In the methanol solution-assisted annealing experiments, two main phases were observed: (I) absorption/swelling when the grating was in the solution and (II) evaporation/shrinkage while the grating was removed from the solution. Figure 20 shows an example of the grating response over time for methanol/water concentrations of 50:50%, 60:40%, and 70:30% v/v. Once the mPOFBGs were immersed in the respective solutions, they immediately started absorbing the solution and getting swollen. This led to some initial red shift for all three cases. However, as soon as the solution started to swell the fibers (which corresponded to their T_g getting lower), the relaxation started to occur. The initial red shift can be seen as the result of a temporary positive balance between the red-shift caused by the solution-mediated swelling due to the solution absorption and the blue-shift induced by the chain alignment relaxation. After this initial lag-phase, the total shift referred to the initial Bragg wavelength became constantly negative and the recorded amount of blue-shift increased very rapidly. The higher the concentration of the methanol, the higher and the faster the relaxation of the fiber was. After the fast Bragg wavelength blue shift, an inflection point in all Bragg wavelength curves was observed and the rate of blue shift gradually became smaller and smaller. When the Bragg wavelength stabilized, the fibers were removed from the solutions. Upon removal, the solution that the fiber absorbed started to evaporate out rapidly. This caused the fiber to shrink further and hence the pitch of the grating was further reduced, leading to an abrupt blue shift. The total amount of blue shift that occurred in three phases for the PMMA mPOFBGs (duplicates) in the experiments at three different solution concentrations is summarized in Table 3. As can be seen from Table 3, the total amount of blue-shift at the end of the experiments increased with the methanol concentration. This proves that the real T_g of PMMA was decreased during the experiments, to an extent that depends on the methanol concentration, in particular increasing with the methanol concentration. The main advantage of this annealing method is that it is cheap compared to the others as it does not require any expensive climate chamber.

Annealing of mPOFBGs has several advantages and is a crucial phase of POFBGs sensor development. By annealing it is possible to fabricate a number of FBGs in a single fiber with a single-phase mask for WDM FBG sensors. In particular, it is possible to obtain an FBG at almost any wavelength with a

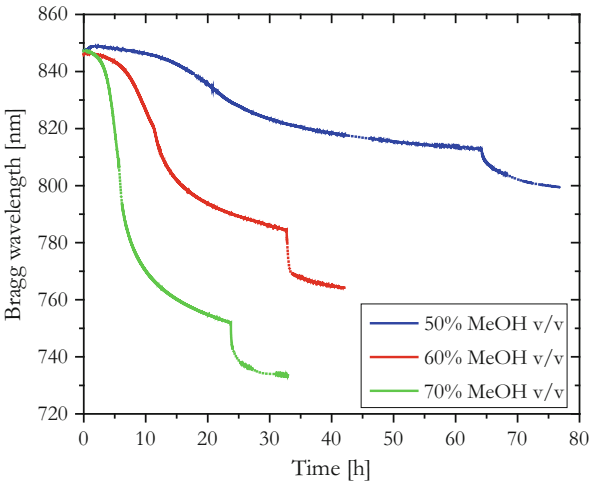

Fig. 20 Bragg wavelengths versus volumetric concentration of methanol (MeOH v/v). Note that the dotted lines indicate the experimental data missing due to high reflection noise and recovered by fitting. The sharp downward jump in the three curves corresponds to the time when the gratings were removed from the respective solutions

Table 3 The total amount of blue shift recorded for the three PMMA mPOFBGs in the three different solution

Methanol:water v/v(%)	Total Bragg wavelength shift (nm)
50:50	−50.0±3.0
60:40	−80.3±2.4
70:30	−111.6±3.2

single-phase mask. Also, annealing results in a linear response of gratings to temperature and humidity and increases the linear operating temperature range of FBGs (Woyessa et al. 2016; Carroll et al. 2007; Johnson et al. 2010b).

Microstructured Polymer Optical Fiber Grating Sensors

Microstructured polymer optical FBGs have been used for the development of various types of sensors such as strain, temperature, humidity, pressure, refractive index, accelerometer. In this section, an overview of the most important sensing applications that mPOFBGs have been employed for is provided.

Strain Sensors

FBGs fabricated in different types of mPOFs have been used for axial strain measurement. The most common way to determine the sensitivity of mPOFBGs to strain in a laboratory environment is by using two 3-D translation stages. First, the fiber is glued on v-grooves mounted on the 3D translation stages with a few centimeters separation from both sides of the grating. One of the translation stages is used to apply axial strain to the fiber (i.e., to the grating) and the other translation stage is used to butt couple light into the mPOF. The strain applied on the grating

Table 4 Strain sensitivity of gratings inscribed in different types of mPOFs and at different wavelengths

Base polymers	Fiber structure/ diameter/core/ hole-to-pitch ratio	Is the grating annealed or not?	Bragg wave-length (nm)	Stain range (%)	Sensitivity (pm/μm)	Temperature at which strain mea-surement is done
PMMA	3 ring hexagonal, 150 μm, 50 μm, MM (Johnson et al. 2010a)	No	827	0–1	0.71	Ambient
	3 ring hexagonal, 130 μm, 9 μm, 0.5 (Stefani et al. 2011)	No	847.6	0–2	0.71	Ambient
			1550		1.3	Ambient
	6 ring hexagonal, 250 μm, 18 μm, 0.52 (Oliveira et al. 2015)	No	1514	0–2	1.65	Ambient
Topas 8007F-04	2 ring hexagonal, 240 μm, 10.2 μm, 0.3 (Yuan et al. 2011)	No	870	0–2.17	0.64	Ambient
Topas 5013S-04	3 ring hexagonal, 130 μm, 9.2 μm, 0.4 (Markos et al. 2013)	Yes, at 80 °C for 3 h	853.4	0–0.3	0.76	50 °C
				0–0.3	0.8	100 °C
				0–0.16	1	110 °C
	3 ring hexagonal, 180 μm, 13 μm, 0.375 (Markos et al. 2013)	No	869.6	0–3	0.75	Ambient
				0–2.2		50 °C
				0–2.5		98 °C
PC	3 ring hexagonal, 150 μm, 7 μm, 0.4 (Fasano et al. 2016)	Yes, at 120 °C for 24 h and at 130 °C for 12 h	875.7	0–3	0.70	Ambient
Zeonex 480R	3 ring hexagonal, 150 μm, 8.8 μm, 0.4 (Woyessa et al. 2017a)	Yes, at 120 °C for 36 h	831.57	0–3	0.77	Ambient

is then determined as the ratio of the elongated length of the fiber at the each strain level to the original length of the fiber defined as the length between the two glue points. By means of this method, strain measurements have been done and sensitivities to strain have been determined to PMMA, Topas 8007S-04, Topas 5013S-04, PC and Zeonex 480R mPOFBGs. Table 4 summarizes the main fiber materials used, whether the fiber is annealed or not before strain measurement, the Bragg grating wavelength region, the strain range, sensitivity to strain, and temperature in which strain measurement was performed.

As it can be seen from Table 4, the strain sensitivity is almost the same for all polymer types as long as the Bragg wavelengths are in the same wavelength region. The PC and the Zeonex mPOFs mentioned in Table 4 were annealed 20 °C below their T_g, and the annealing process was stopped when the blue shift saturated and shows a wider range of strain sensing up to 3%. Moreover, it can be seen that the sensitivity to strain is also dependent on the Bragg wavelength. Grating inscribed at 1550 nm region have about two times better sensitivity than those at 850 nm; nonetheless the propagation loss of POFs is higher in 1550 nm region.

Temperature Sensors

As mPOFBGs have been used to measure axial strain they have been also used to gauge temperature. The temperature operating range of mPOFBGs varies depending on the T_g of the base polymer material used to fabricate the fibers. The two most common setups used to characterize mPOFBGs are heating elements and climate chambers. In the former case, an mPOFBG is placed near the heating element and the temperature close to the grating is monitored by a thermocouple. Despite this characterization setup is cost effective; its major limitation is that the humidity in the vicinity of grating is uncontrolled. This causes a significant error particularly when the characterization involves FBGs fabricated from polymers that have affinity to water such as PMMA. This is due to the fact that humidity decreases as temperature increases and leading an additional blue shift of the Bragg wavelength. Characterizing the mPOFBGs in terms of temperature in a climate chamber is probably the best way to perform accurate thermal characterization of the sensor as the humidity is more accurately controlled and the resulting error is minimized. Table 5 summarizes the fiber materials used, whether the fiber is annealed or not before the temperature characterization, the Bragg wavelength region, the temperature range, sensitivity to temperature, setup used, and RH at which the temperature measurement was performed.

As can be seen from Table 5, unlike the strain sensitivity the temperature sensitivities of the gratings showed significantly variation, even for the same wavelength region. This inconsistent response can be attributed to several reasons such as different characterization setups employed, whether the grating is annealed or not and so on. Among the currently existing POFBGs, PC-based mPOFBGs are able to measure the highest temperature, i.e., up to 125 °C.

Humidity Sensors

Some of the polymers that they have been used to fabricate POFs have moisture absorbing capabilities. PMMA and PC are, for instance, humidity-sensitive polymers. When moisture is absorbed in mPOFs based on these polymers, two important phenomena occur in the fiber: a change in its size (length and diameter) and refractive index. Because the Bragg wavelength depends on both the

Table 5 Temperature sensitivity of gratings inscribed in different types of mPOFs and at different wavelengths

Base polymers	Fiber structure/diameter/core/hole-to-pitch ratio	Is the grating or fiber annealed or not?	Bragg wavelength (nm)	Temperature range (°C)	Sensitivity (pm/°C)	Set up	Humidity at which temperature measurement is done
PMMA	4 ring hexagonal, 150 μm, 14.6 μm, 0.3 (Carroll et al. 2007)	Yes, at 80 °C for 7 h	1560	20–89	52	Heating element	Ambient
Topas 8007F-04	2 ring hexagonal, 240 μm, 10.2 μm, 0.33 (Yuan et al. 2011)	No	870	23.5–32.6	−78	Heating element	Ambient
	2 ring hexagonal, 270 μm, 13.2 μm, 0.45 (Yuan et al. 2011)	No	1567.9	20–35	−36.5	Climate chamber	55% RH
Topas 5013S-04	3 ring hexagonal, 130 μm, 9.2 μm, 0.4 (Markos et al. 2013)	Yes, at 80 °C for 3 h	853.4	24–107	−14.46	Heating element	Ambient
Polycarbonate	3 ring hexagonal, 150 μm, 7 μm, 0.4 (Fasano et al. 2016)	Yes, at 120 °C for 24 h and at 130 °C for 12 h	875.7	23–125	−29.99 ± 0.17	Heating element	Ambient
	3 ring hexagonal, 125 μm, 10 μm, 0.4 (Woyessa et al. 2017b)	Yes 125 °C for 36 hr	880.19	20–100	−25.67 ± 0.6	Climate chamber	50%, 90% RH
Zeonex 480R	3 ring hexagonal, 150 μm, 8.8 μm, 0.4 (Woyessa et al. 2017a)	Yes, at 120 °C for 36 h	831.57	20–100	−24.01 ± 0.1	Climate chamber	50% RH

period of the grating and refractive index, when moisture is absorbed, the Bragg wavelength is consequently directly affected. By exploiting this crucial property of such polymers, mPOFBG humidity sensors have been developed. It is very important here to emphasize that PMMA and PC mPOFBGs are also sensitive to temperature. Therefore, when such mPOFBGs are used as humidity sensors, cross sensitivity to temperature affects the humidity response of the grating and vice versa. Woyessa et al. showed that in order to achieve temperature independent humidity responses, mPOFBGs have to be annealed not only at temperature close to the T_g of the polymer but also at high RH (Woyessa et al. 2016). For instance, at 80 °C and 90% RH for PMMA-based fibers to operate up to 75 °C and 90% RH with no hysteresis. Annealing the fiber at these conditions not only helps to develop temperature insensitive humidity sensor but also makes the sensor more stable, hysteresis free, and highly sensitive to humidity. PMMA mPOFBGs that have not been annealed or annealed at a very low RH, for instance, in a conventional oven, showed low sensitivity, highly temperature-dependent sensitivity, and highly nonlinear response to humidity. Figure 21a and b depicts how the response to humidity of PMMA mPOFBGs is highly affected by the RH level.

As it can be seen from Fig. 21a, only the mPOFBG that was annealed up to 90% RH at 80 °C exhibited the most stable response to humidity in the range 10–90%RH up to 75 °C. In contrast, the PMMA mPOFBGs annealed at a lower humidity showed a smaller sensitivity with hysteresis at 25 °C and 50 °C. Moreover, at 75 °C they showed a fast and high nonlinear decrease in the Bragg wavelength when the RH was raised just above the annealing RH level, as can be seen in Fig. 21b. The sensitivity to humidity for mPOFBG annealed up to 90% RH was around 35 pm/% RH for the whole range of operating temperature at a Bragg wavelength of 600 nm. It is possible to get a higher sensitivity if the Bragg wavelength falls within a longer wavelength yet still low loss region, such as the 850 nm region. To achieve this, rather than annealing the fiber after inscription and shifting the grating to shorter wavelength, the fiber can be annealed before inscription. Figure 22a and b shows the humidity response of a PMMA mPOFBG inscribed in a fiber that was annealed at 80 °C and 90% RH for 36 h before inscription. The humidity sensitivity of this grating was 45 pm/ %RH which is 10 pm/ % RH higher than the response measured at 600 nm Bragg grating wavelength.

However, considering that there are applications that require humidity measurements at temperatures beyond the one PMMA mPOFBGs can operate at, PC mPOFBGs humidity sensors have been developed instead. Polycarbonate has also moisture absorbing capability although it is not as strong as PMMA. The water absorption (saturation value) at 23 °C of PC is 0.3% (Optical properties of Makrolon and Apec 2014), whereas that of PMMA is 2.1% (GEHR PMMA (Acrylic), http://www.gehrplastics.com/pmma-acrylic.html). PC mPOFBGs were demonstrated to be able to measure RH in the range from 10% to 90% up to 100 °C. It is possible to operate PC mPOFBG beyond this temperature level as the T_g of PC is 145 °C, but the climate chamber used to measure humidity operates only up to 100 °C. The measured humidity sensitivity of PC mPOFBGs was 7.25 ± 0.08 pm/% RH

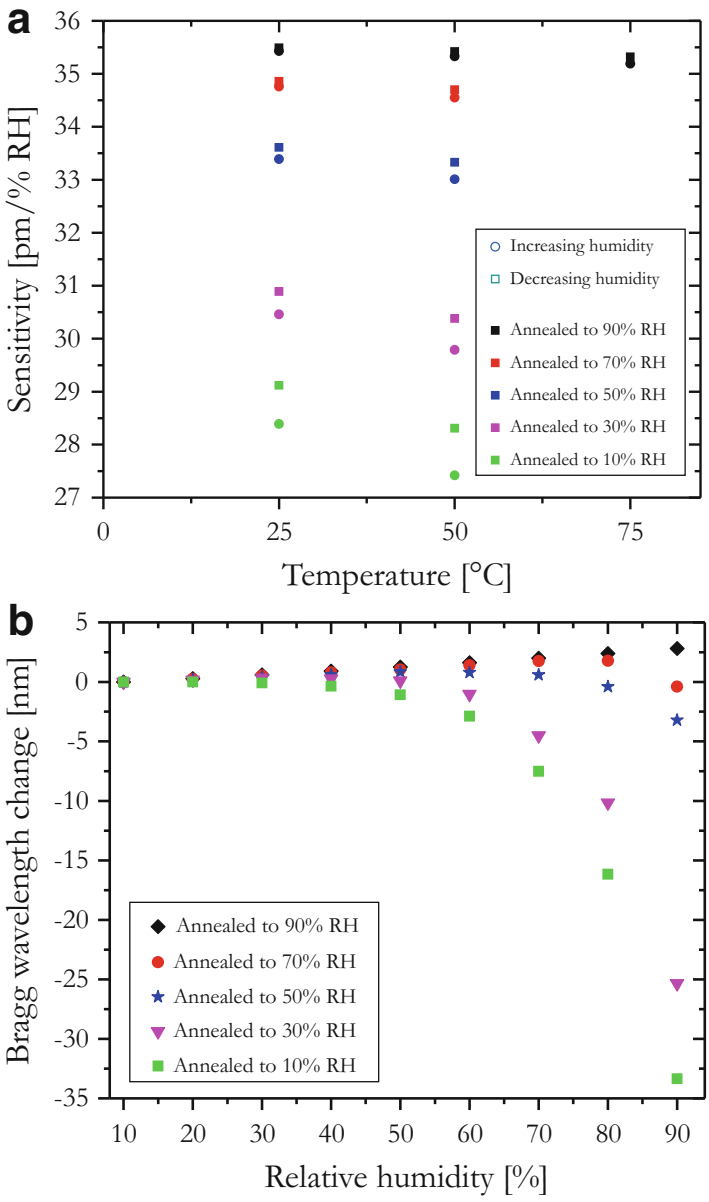

Fig. 21 (**a**) Humidity sensitivity of PMMA mPOFBGs annealed up to 90%, 70%,50%, 30%, and 10% RH at 25 °C and 50 °C and PMMA mPOFBG annealed to 90% at 75 °C. (**b**) Humidity responsivity of PMMA POFBGs annealed up to 90%, 70%, 50%, 30%, and 10% RH at 75 °C (Woyessa et al. 2016)

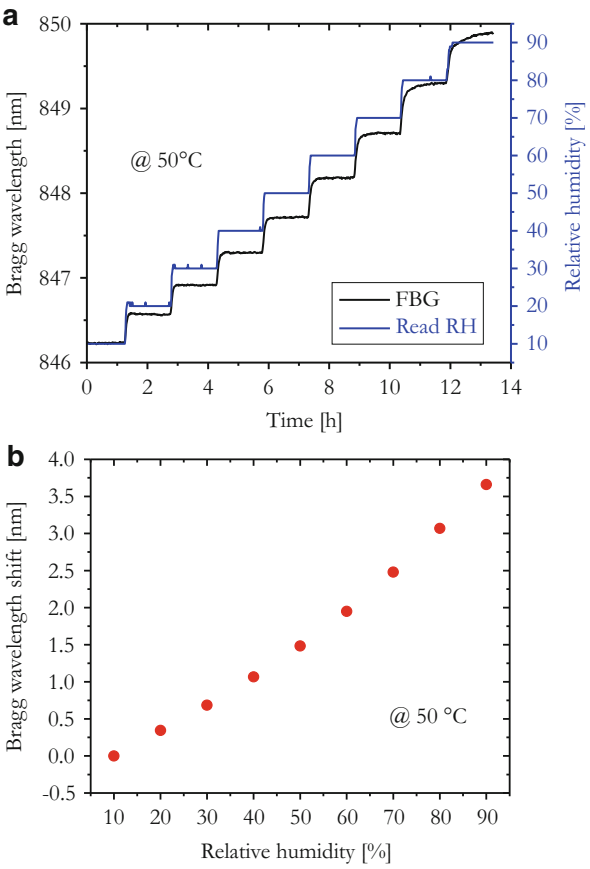

Fig. 22 (**a**) Humidity response of PMMA mPOFBG at 50 °C in the 850 nm region where the fiber annealed at 80 °C and 90% RH for 36 h before the grating inscription. (**b**) The corresponding stabilized response of the grating

in the range 10–90% RH at 100 °C. Polycarbonate mPOFBGs can be operated well beyond the PMMA mPOFBG operating temperature limit, but at the cost of having lower sensitivity than PMMA one. The RH sensitivity of PC mPOFBGs is indeed 7 times smaller than PMMA mPOFBGs. Despite the fact that the low moisture absorption property of PC can be considered as a limitation in humidity sensitivity, this turns out to be an advantage when a temperature measurement is performed. For instance, for a climate chamber that has RH precision of an order of 1% when PMMA mPOFBGs are characterized with regard to their temperature response, a single % of RH fluctuation in the chamber makes the temperature measurement very difficult as PMMA mPOFBGs are highly sensitive to humidity. Figure 23 shows the temperature response of PMMA mPOFBGs at 50% RH (set value). As it can be seen from the figure, it is hardly possible to get accurate temperature measurement due to 1% fluctuation in RH. In addition, PMMA mPOFBGs have a lower temperature sensitivity compared to PC mPOFBGs (Woyessa et al. 2017b).

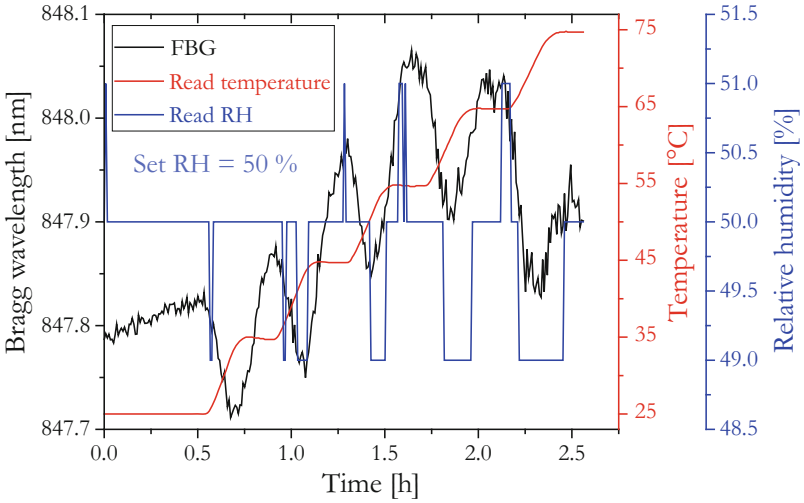

Fig. 23 Temperature responses of PMMA mPOFBGs at 50% RH. The fibers were annealed at 80 °C and 90% RH for 36 h before the grating inscription

This problem was not seen when temperature characterization was done for PC mPOFBG. This is due to the fact that PC has smaller moisture absorption capability, so that 1% RH fluctuation in the chamber does not affect the temperature response of the PC grating significantly. The temperature response of the PC mPOFG can be seen from Fig. 24a and b. Therefore, a more precise climate chamber is required to accurately calibrate the temperature response of PMMA mPOFBGs.

Pressure Sensors

Hydrostatic pressure is one of the most commonly monitored measurands in many applications. Microstructured polymer optical FBGs have been used to develop hydrostatic pressure sensors. Johnson et al. demonstrated the first hydrostatic pressure sensors using MM PMMA mPOFBGs (Johnson et al. 2012). The principle behind measuring hydrostatic pressure of the environment using mPOFBGs relies upon two factors. When the hydrostatic pressure of the environment in which the grating is exposed increases, the mPOF shrinks. Thus, the pitch of the grating decreases and this leads to a negative Bragg wavelength shift. The other effect relies upon the strain optic effect of the fiber which increases as the fiber is compressed resulting in a positive Bragg wavelength shift. The setup used by Johnson et al. to determine the hydrostatic pressure response of mPOFBG is shown in Fig. 25. The fiber used in their experiments was purely made from PMMA and had a core and an outer diameter of 50 μm and 150 μm, respectively. They measured pressure up 10 MPa (100 bar). The grating had a Bragg wavelength of 1561.5 nm

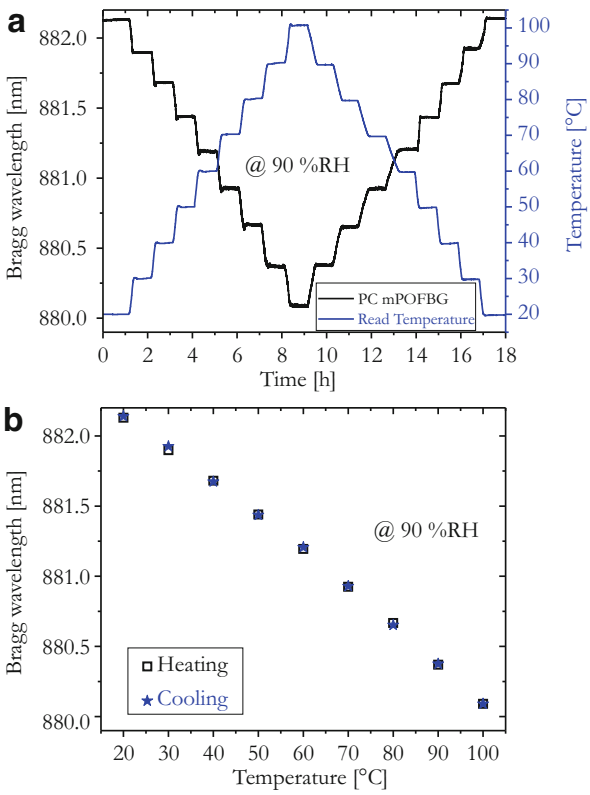

Fig. 24 (**a**) Temperature responses of PC mPOFBGs at 90% RH. (**b**) The corresponding stabilized temperature response where data points are taken at the end of each stabilization period (Woyessa et al. 2017b)

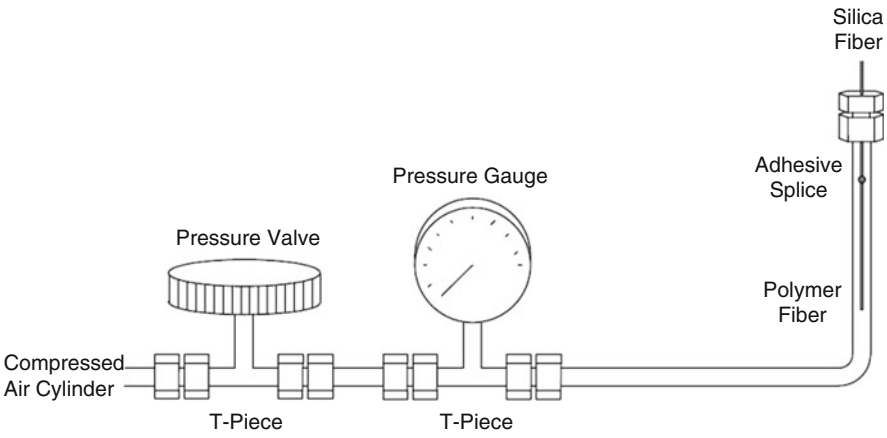

Fig. 25 Experimental setup to characterize the hydrostatic pressure responsivity of MM PMMA mPOFBG (Johnson et al. 2012)

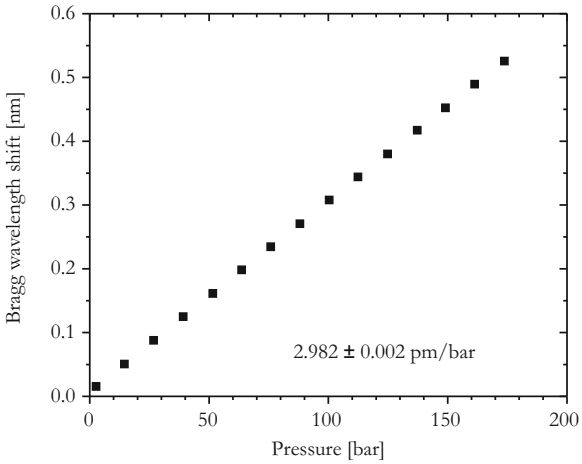

Fig. 26 Hydrostatic pressure response of a humidity insensitive single mode mPOFBG

with FWHM of 8.78 nm. In the experiment, it was seen that a ± 2 °C reversible temperature fluctuation when the pressure was ramped up from atmospheric to 10 MPa. By increasing the pressure from 2 MPa to 10 MPa with a step of by 1 MPa, a pressure sensitivity of 100 ± 9.38 pm/MPa was obtained. A similar experiment done on silica FBG with a Bragg wavelength of 1551.04 nm with FWHM of 0.22 nm gave a sensitivity of −3.88 ± 0.04 pm/MPa. This result showed that the MM mPOFBG was 25 times more sensitive than the silica FBG.

In 2016 Pedersen et al. demonstrated hydrostatic pressure sensor with humidity insensitive single-mode mPOFBGs up to 20 MPa (200 bar) (Pedersen et al. 2016). In their experiment in order to avoid the fluctuation of temperature and its effect on the pressure response of the FBG while the pressure was ramped up and down, the measurement was done in a gas free environment with the FBG saturated with water. As a result, the fluctuation in temperature was limited to only ±0.2 °C, which was around ±2 °C in Johnson et al.'s experiments. The grating used in their experiment had a Bragg wavelength of 865 nm with FWHM of 1 nm. The pressure sensitivity of the grating was 29.82 ± 0.02 pm/MPa with a resolution of 0.2 MPa. The response of the grating with pressure is shown in Fig. 26.

Acceleration Sensors

Microstructured polymer optical FBG sensors have also found application in the development of accelerometers. Stefani et al. demonstrated the first mPOFBG accelerometer both in the 850 nm and 1550 nm wavelength regions (Stefani et al. 2012b). The schematic diagram of the experimental setup for the characterization of the mPOFBG-based accelerometer is shown in Fig. 27. In this system, the acceleration was converted into strain by a mechanical transducer. The transducer was made in such way that the strain on the fiber was linearly

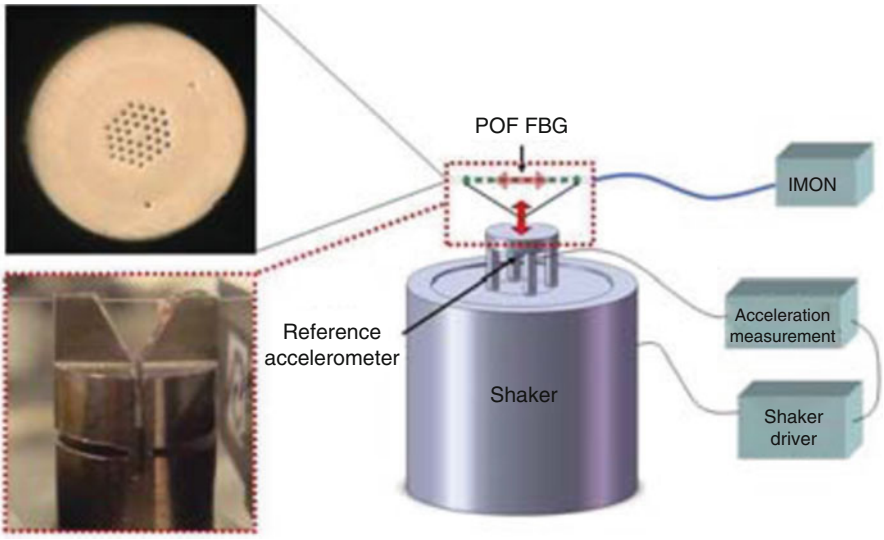

Fig. 27 Schematic of the accelerometer characterization setup. Top inset: mPOF cross section. Bottom inset: mPOF FBG-based accelerometer (Stefani et al. 2012b)

Table 6 The acceleration sensitivity of PMMA mPOFBGs and silica FBGs for two different fiber diameters and wavelength regions

Fiber type	Fiber diameter (μm)	Bragg wavelength (μm)	Sensitivity (pm/g)
PMMA mPOF	130	1550	15.2
Step index silica	80	1550	5.1
PMMA mPOF	130	850	5.9
Step index silica	125	850	1.8

dependent on the acceleration. Therefore, the fiber sensor was calibrated in way that the amount of the Bragg wavelength shift corresponded to certain levels of acceleration.

The gratings were fabricated from PMMA mPOFs with a hole to pitch ratio of 0.5 by using the phase mask technique. The phase masks had a pitch of 1024.7 nm for the 1550 nm FBGs and a pitch of 572.4 nm for the 850 nm FBGs. In their experiments, the Bragg wavelength change versus acceleration at a fixed frequency of 159.2 Hz was measured in the range from 0.1 g to 15 g acceleration. An acceleration of 15 g corresponded to a strain of 0.02%. POFs exhibit a larger linear strain operation range and thus can measure very high accelerations. The demonstration here was limited to only 15 g because of the shaker limit. For comparison purpose, the same experiment was repeated with silica FBGs in the same wavelength regions. The resulting sensitivities are summarized in Table 6. The response was found to be linear for both mPOF and silica. However, the mPOF displayed sensitivity three times higher than that of silica.

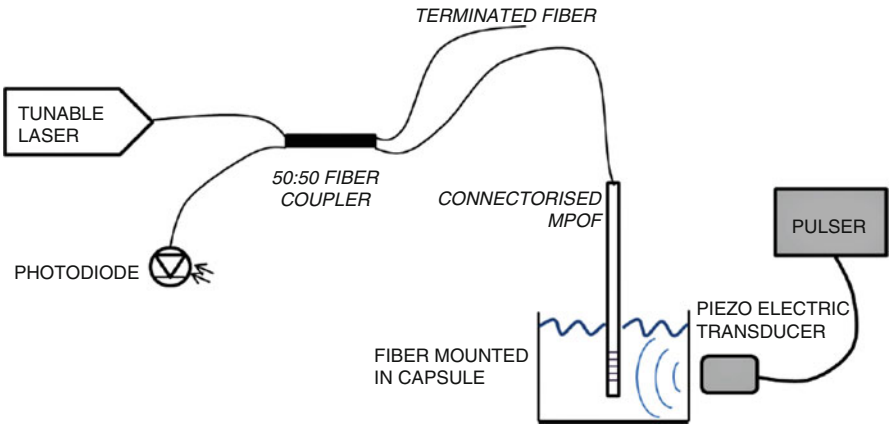

Fig. 28 Experimental setup for the ultrasonic detection experiments using PMMA mPOFBGs (Broadway et al. 2015)

Biomedical Sensor

One of the unique properties of polymers is their biocompatibility and mPOFBGs have been considered as potential candidate in biomedical areas such as for the detection of ultrasonic waves (Markos et al. 2011; Jensen et al. 2005; Emiliyanov et al. 2007; Broadway et al. 2015). Biocompatibility constitutes an important property for optoacoustic endoscopy. For endoscopic applications, one of the most important criteria is the size of the sensor, as the sensor has to be inserted in a cavity. In addition, high sensitivity is also required. The basic principle behind using mPOFBGs for ultrasonic wave detection again relies on the strain effect. The mPOFBGs have already proved to be highly sensitive to strain, and this makes them particularly suitable for optoacoustic endoscopy. The characterization setup used for the detection of ultrasonic waves in the laboratory is depicted as in Fig. 28 (Broadway et al. 2015).

First, the grating profile was examined by using a broadband light source and an OSA to determine the 3 dB point of the grating. Then the broadband source and the spectrum analyzer were replaced by a tunable laser and photodetector connected with an oscilloscope, respectively. The laser was then tuned to the 3 dB point of the mPOFBG. Therefore, when the ultrasonic wave perturbed the grating, the Bragg wavelength shifted and led to an amplitude variation at the detector output, which was then observed on the oscilloscope. In order to generate an ultrasonic wave, piezo electric transducer was used. A transducer was added to the setup and acoustically coupled using water as the acoustic medium. Figure 29 shows a typical ultrasonic response of PMMA mPOFBG immersed in water (acoustic medium) using transducers at 1, 5, and 10 MHz. Therefore, by this method a compact in-fiber ultrasonic detector based on mPOFBGs was developed.

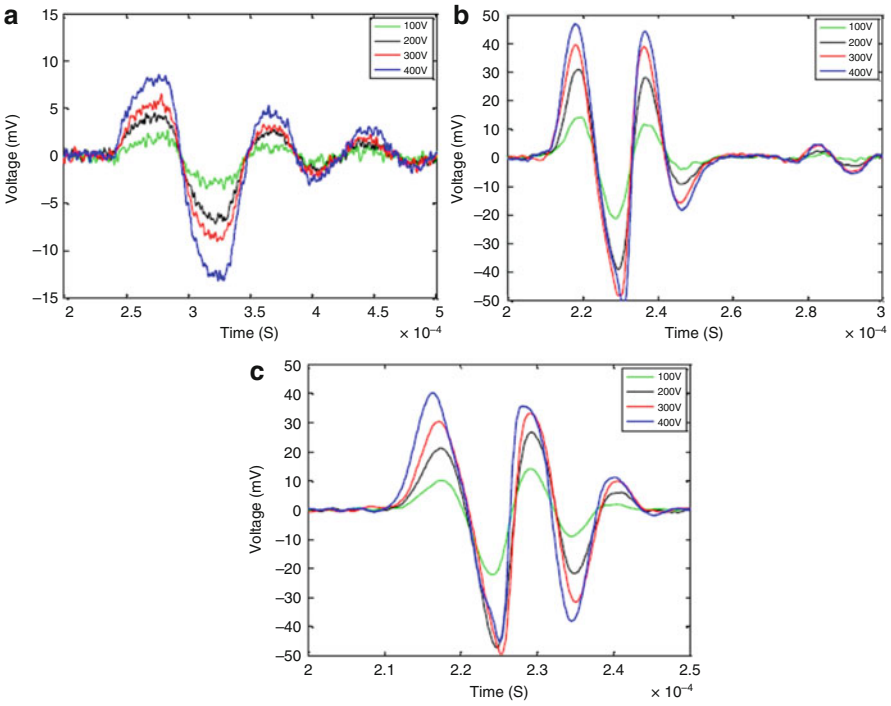

Fig. 29 Ultrasonic response PMMA mPOFBG for (**a**) 1 MHz, (**b**) 5 MHz, and (**c**) 10 MHz at excitation voltages between 100 and 400 V (Broadway et al. 2015)

Thermo-Hygrometer

Grating fabricated in a specially designed mPOF has been proposed by Woyessa et al. towards the development of a novel thermo-hygrometer (Woyessa et al. 2017c). The fiber was fabricated from two polymer materials and involved an over cladding as well. The core and the cladding of the fiber consisted of Zeonex 480R and PMMA over cladding (see Fig. 30). The sensing probe was based on two separate in-line FBGs inscribed in the fabricated mPOF. To inscribe the two gratings, only a single-phase mask was used in combination with thermal annealing technique.

In a piece of the fabricated fiber, at one end, the PMMA over cladding was etched out for few centimeters and the first grating was inscribed in the etched section of the fiber. Then the grating was annealed to shift the Bragg wavelength by few nanometers and followed by inscribing the second grating in the unetched section of the fiber few centimeters away from the first grating. The gratings configuration and spectrum is depicted in Fig. 31a and b, respectively.

The materials used for the sensor fabrication have different properties. PMMA has very high affinity to water, whereas Zeonex has a very small moisture absorbing capability (Woyessa et al. 2016, 2017a). Thus, the basic principle behind humidity

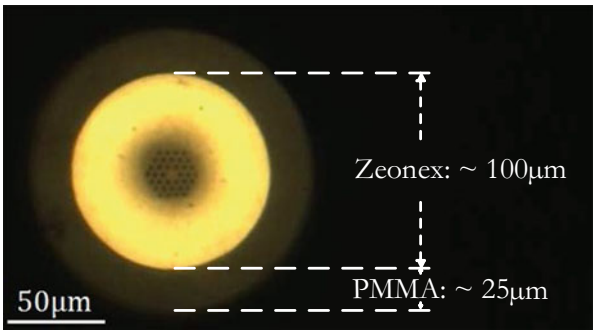

Fig. 30 Zeonex core and cladding and PMMA over-cladding mPOF

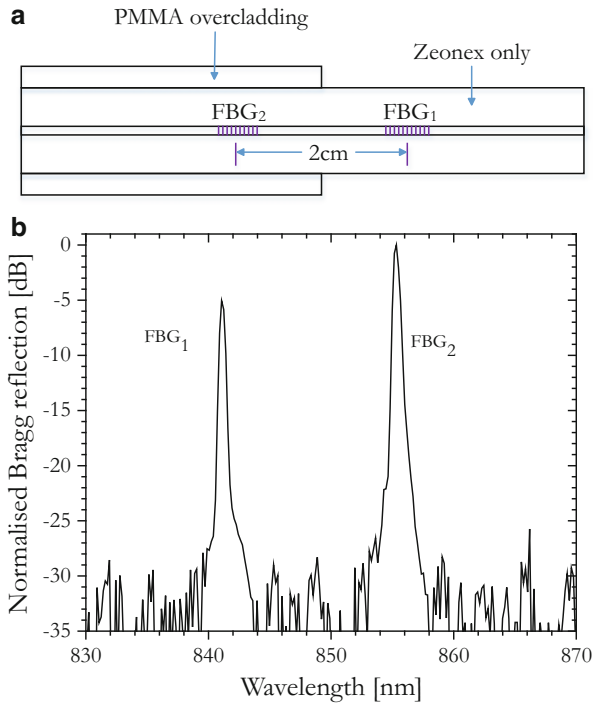

Fig. 31 Dual gratings (**a**) Configuration (**b**) reflection spectrum

measurement with the PMMA over cladding Zeonex mPOF relies on the swelling effect caused by PMMA. When PMMA absorbs moisture, it induces strain on the grating inscribed in the Zeonex core thus effectively leading to a shift in the Bragg wavelength. The temperature and the relative humidity response of the dual gratings are shown in Fig. 32a and b, respectively.

The responses of the two gratings are modeled as:

$$\Delta\lambda_1 = \alpha_1 \Delta T + \beta_1 \Delta H \tag{6}$$

$$\Delta\lambda_2 = \alpha_2 \Delta T + \beta_2 \Delta H + \gamma_2 \Delta H_2 \tag{7}$$

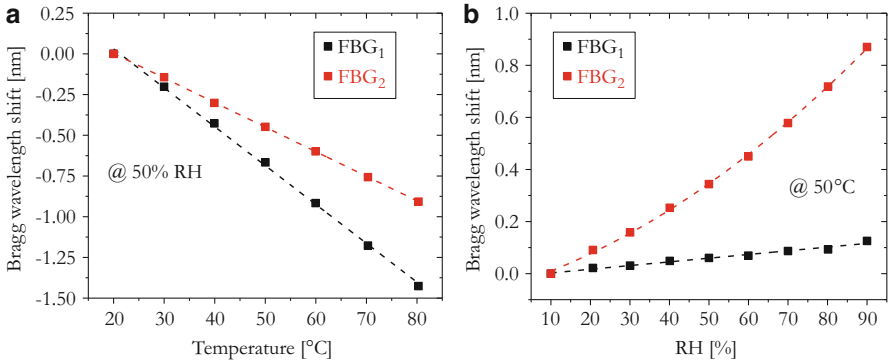

Fig. 32 (**a**) The temperature response of FBG_1 and FBG_2 at 50% RH. The dashed lines correspond to the linear fitting of the data. (**b**) The humidity response of FBG_1 and FBG_2 at 50 °C. The dashed lines correspond to a linear fit of FBG_1 data and a second-order polynomial fit of FBG_2 data

Table 7 Standard Errors of the Fitting Parameters

i	α_i (pm/°C)	β_i(Pm/% RH)	γ_i(Pm/% $(RH)^2$)
1	-23.9 ± 0.4	1.4 ± 0.1	–
2	-15.1 ± 0.1	6.4 ± 0.5	0.057 ± 0.004

where $\Delta\lambda_1$ and $\Delta\lambda_2$ are the Bragg wavelength shifts of FBG_1 and FBG_2, respectively, as a result of changes in RH ΔH and temperature ΔT and the coefficients α_i, β_i, and γ_i are listed in Table 7, which are determined by fitting the polynomial equations, Eqs. 6 and 7, to the calibration data.

These coefficients are used to reconstruct the values of temperature and relative humidity from the wavelength and in the range 10–90% RH and 20–80 °C, a root mean square deviation of 0.8% RH and 0.6 °C was found. These investigations showed that the proposed sensor system is a viable way of effectively separating the responses to temperature and humidity. The potential advantages of the developed device are being easy to fabricate, low cost, compact, all polymer based, and mechanically stable. In addition, it has also multiplexing capability as the two gratings are very close in wavelength.

Conclusion

In conclusion, this chapter overviewed the most important efforts from several research groups around the globe to develop FBG-based optical sensors using mPOFs. Initially the main three different FBG inscription techniques (interferometric, phase-mask, and point-by-point) based on different inscription lasers (CW UV, pulsed UV, near-IR lasers) are presented and directly compared. Then the crucial impact of microstructured cladding of a fiber on the inscription process for the development of high-quality FBGs was discussed. The main results reported so far regarding the optimal conditions in terms of angle and orientation of the mPOF

during the inscription are also summarized. Section "Microstructured Polymer Optical Fiber Bragg Gratings" focused on how different polymer materials, such as PMMA, Topas, Zeonex and PC, that have been so far used for the development of novel mPOFBGs suitable for many environmental measurands monitoring applications, significantly extending their functionality in several sensing applications. In the last section, different case studies utilizing mPOFBGs towards the development of strain, temperature, humidity, pressure, acceleration, biomedical sensors as well thermo-hygrometer are discussed.

Acknowledgements The authors would like to acknowledge the People Programme (Marie Curie Actions) of the European Union's Seventh Framework Programme FP7/2007-2013/ under REA grant agreement n° 608382 and Danish Council for Independent Research (FTP Case No. 4184-00359B).

References

T. Baghdasaryan, T. Geernaert, F. Berghmans, H. Thienpont, Geometrical study of a hexagonal lattice photonic crystal fiber for efficient femtosecond laser grating inscription. Opt. Express **19**(8), 7705–7716 (2011)

T. Bremner, A. Rudin, D.G. Cook, Melt flow index values and molecular weight distributions of commercial thermoplastics. J. Appl. Polym. Sci. **41**(78), 1617–1627 (1990)

C. Broadway, D. Gallego, G. Woyessa, A. Pospori, O. Bang, D.J. Webb, G. Carpintero, H. Lamela, in Polymer optical fibre sensors for endoscopic opto-acoustic imaging, *Proceedings of SPIE 9539, Opto-Acoustic Methods and Applications in Biophotonics II*, 953907 (2015)

I.-L. Bundalo, K. Nielsen, C. Markos, O. Bang, Bragg grating writing in PMMA microstructured polymer optical fibers in less than 7 minutes. Opt. Express **22**(5), 5270–5276 (2014)

I.-L. Bundalo, K. Nielsen, O. Bang, Angle dependent fiber Bragg grating inscription in microstructured polymer optical fibers. Opt. Express **23**(3), 3699–3707 (2015)

K.E. Carroll, C. Zhang, D.J. Webb, K. Kalli, A. Argyros, M.C.J. Large, Thermal response of Bragg gratings in PMMA microstructured optical fibers. Opt. Express **15**(14), 8844–8850 (2007)

Data Sheet Topas 5013S-04, Topas Advanced Polymers Inc., 2015, http://www.topas.com/sites/default/files/TDS_5013S_04_e_1.pdf

Data Sheet Topas 8007F-04, Topas Advanced Polymers Inc., 2015, http://www.topas.com/sites/default/files/TDS_8007F-04_english%20units_0.pdf

H. Dobb, D.J. Webb, K. Kalli, A. Argyros, M.C.J. Large, M.A. van Eijkelenborg, Continuous wave ultraviolet light-induced fiber Bragg gratings in few- and single-mode microstructured polymer optical fibers. Opt. Lett. **30**(24), 3296–3298 (2005)

G. Emiliyanov, J.B. Jensen, O. Bang, P.E. Hoiby, L.H. Pedersen, E.M. Kjaer, L. Lindvold, Localized biosensing with Topas microstructured polymer optical fiber. Opt. Lett. **32**(5), 460–462 (2007)

A. Fasano, G. Woyessa, P. Stajanca, C. Markos, A. Stefani, K. Nielsen, H.K. Rasmussen, K. Krebber, O. Bang, Fabrication and characterization of polycarbonate microstructured polymer optical fibers for high temperature resistant fiber Bragg grating strain sensors. Opt. Mater. Express **6**(2), 649–659 (2016)

A. Fasano, G. Woyessa, J. Janting, H.K. Rasmussen, O. Bang, Solution-mediated annealing of polymer optical fiber Bragg gratings at room temperature. IEEE Photon. Technol. Lett. **29**(8), 687–690 (2017)

GEHR PMMA (Acrylic), http://www.gehrplastics.com/pmma-acrylic.html

K.O. Hill, B. Malo, F. Bilodeau, D.C. Johnson, J. Albert, Bragg gratings fabricated in monomode photosensitive optical fibre by UV exposure through a phase mask. Appl. Phys. Lett. **62**(10), 1035–1037 (1993)

X. Hu, G. Woyessa, D. Kinet, J. Janting, K. Nielsen, O. Bang, C. Caucheteur, BDK-doped core microstructured PMMA optical fiber for effective Bragg grating photo-inscription. Opt. Lett. **42**(11), 2206–2212 (2017)

T. Ishigure, M. Hirai, M. Sato, Y. Koike, Graded-index plastic optical fiber with high mechanical properties enabling easy network installations. II. J. Appl. Polym. Sci. **91**(1), 404–409 (2004)

J. Jensen, P. Hoiby, G. Emiliyanov, O. Bang, L. Pedersen, A. Bjarklev, Selective detection of antibodies in microstructured polymer optical fibers. Opt. Express **13**(15), 5883–5889 (2005)

I.P. Johnson, K. Kalli, D.J. Webb, 827 nm Bragg grating sensor in multimode microstructured polymer optical fibre. Electron. Lett. **46**(17), 1217–1218 (2010a)

I.P. Johnson, D.J. Webb, K. Kalli, M.C.J. Large, A. Argyros, Multiplexed FBG sensor recorded in multimode microstructured polymer optical fiber. Proc. SPIE **7714**, 77140D (2010b)

I.P. Johnson, W. Yuan, A. Stefani, K. Nielsen, H.K. Rasmussen, L. Khan, D.J. Webb, K. Kalli, O. Bang, Optical fibre Bragg grating recorded in TOPAS cyclic olefin copolymer. Electron. Lett. **47**(4), 271–272 (2011)

I.P. Johnson, D.J. Webb, K. Kalli, Hydrostatic pressure sensing using a polymer optical fiber Bragg gratings. Proc. SPIE **8351**, 835106 (2012)

K. Kalli, C. Riziotis, A. Posporis, C. Markos, C. Koutsides, S. Ambran, A.S. Webb, C. Holmes, J.C. Gates, J.K. Sahu, P.G.R. Smith, Flat fibre and femtosecond laser technology as a novel photonic integration platform for optofluidic based biosensing devices and lab-on-chip applications: Current results and future perspectives. Sens. Actuators B. Chem. **209**, 1030–1040 (2015)

G. Khanarian, H. Celanese, Optical properties of cyclic olefin copolymers. Opt. Eng. **40**(6), 1024–1029 (2001)

S.G. Leon-Saval, R. Lwin, A. Argyros, Multicore composite single-mode polymer fiber. Opt. Express **20**(1), 141–148 (2012)

B. Malo, K.O. Hill, F. Bilodeau, D.C. Johnson, J. Albert, Point-by-point fabrication of micro-Bragg grating in photosensitive fibre using single excimer pulse refractive index modification techniques. Electron. Lett. **29**(18), 1668–1669 (1993)

C. Markos, W. Yuan, K. Vlachos, G.E. Town, O. Bang, Label-free biosensing with high sensitivity in dual-core microstructured polymer optical fibers. Opt. Express **19**(8), 7790–7798 (2011)

C. Markos, A. Stefani, K. Nielsen, H.K. Rasmussen, W. Yuan, O. Bang, High-Tg TOPAS microstructured polymer optical fiber for fiber Bragg grating strain sensing at 110 degrees. Opt. Express **21**(4), 4758–4765 (2013)

G.D. Marshall, D.J. Kan, A.A. Asatryan, L.C. Botten, M.J. Withford, Transverse coupling to the core of a photonic crystal fiber: The photo-inscription of gratings. Opt. Express **15**(12), 7876–7887 (2007)

A. Martinez, M. Dubov, I. Khrushchev, I. Bennion, Direct writing of fibre Bragg gratings by femtosecond laser. Electron. Lett. **40**(19), 1170–1172 (2004)

G. Meltz, W.W. Morey, W.H. Glenn, Formation of Bragg gratings in optical fibres by a transverse holographic method. Opt. Lett. **14**(15), 823–825 (1989)

R. Oliveira, L. Bilro, R. Nogueira, Bragg gratings in a few mode microstructured polymer optical fiber in less than 30 seconds. Opt. Express **23**(8), 10181–10187 (2015)

Optical properties of Makrolon and Apec for non-imaging optics, Bayer Material ScienceAG, 2014, http://www.plastics.covestro.com/Products/~/media/B6555362438341FF9804F21A253E5B23.ashx?la=en

J.K.M. Pedersen, G. Woyessa, K. Nielsen, O. Bang, Intrinsic pressure response of a single-mode cyclo olefin polymer microstructured optical fibre Bragg grating, in *Proceedings of the International Plastic Optical Fibres Conference, Birmingham* (2016). ISBN: 978 1 85449 408 5

S. Roy, C.Y. Yue, Z.Y. Wang, L. Anand, Thermal bonding of microfluidic devices: Factors that affect interfacial strength of similar and dissimilar cyclic olefin copolymers. Sens. Actuators B Chem. **161**(1), 1067–1073 (2012)

D. Sáez-Rodríguez, K. Nielsen, H.K. Rasmussen, O. Bang, D.J. Webb, Highly photosensitive polymethyl methacrylate microstructured polymer optical fiber with doped core. Opt. Lett. **38**(19), 3769–3772 (2013)

E.E. Shafee, Effect of photodegradation on the [beta]-relaxation in poly(methylmethacrylate). Polym. Degrad. Stab. **53**, 57–61 (1996)

L.S.A. Smith, V. Schmitz, The effect of water on the glass transition temperature of poly (methyl methacrylate). Polymer **29**(10), 1871–1878 (1988)

G. Statkiewicz-Barabach, K. Tarnowski, D. Kowal, P. Mergo, W. Urbanczyk, Fabrication of multiple Bragg gratings in microstructured polymer fibers using a phase mask with several diffraction orders. Opt. Express **21**(7), 8521–8534 (2013)

A. Stefani, W. Yuan, C. Markos, O. Bang, Narrow bandwidth 850 nm fiber Bragg gratings in few-mode polymer optical fibers. IEEE Photon. Technol. Lett. **23**(10), 660–662 (2011)

A. Stefani, M. Stecher, G.E. Town, O. Bang, Direct writing of fiber Bragg grating in microstructured polymer optical fiber. IEEE Photon. Technol. Lett. **24**(13), 1148–1150 (2012a)

A. Stefani, S. Andresen, W. Yuan, N. Herholdt-Rasmussen, O. Bang, High sensitivity polymer optical fiber-Bragg-grating-based accelerometer. IEEE Photon. Technol. Lett. **24**(9), 763–765 (2012b)

Technical data, Zeonex, Cyclo Olifen Polymer (COC), 2017, http://www.zeonex.com/optics.aspx

Topas COC product overview, Topas Advanced Polymers Inc., 2014, http://www.topas.com/sites/default/files/files/TOPAS_Brochure_E_2014_06(1).pdf

É. Torres, M.N. Berberan-Santos, M.J. Brites, Synthesis, photophysical and electrochemical properties of perylene dyes. Dyes Pigments **112**, 298–304 (2015)

D.L. Williams, Photosensitivity: The phenomenon and its applications, *Advanced Photonic Topics*, (Universidad de Cantabria, Santander, 1997). books.google.com

D.R.G. Williams, P.E.M. Allen, V.T. Truong, Glass transition temperature and stress relaxation of methanol equilibrated poly (methyl methacrylate). Eur. Polym. J. **22**(11), 911–919 (1986)

G. Woyessa, K. Nielsen, A. Stefani, C. Markos, O. Bang, Temperature insensitive hysteresis free highly sensitive polymer optical fiber Bragg grating humidity sensor. Opt. Express **24**(2), 1206–1213 (2016)

G. Woyessa, A. Fasano, C. Markos, A. Stefani, H.K. Rasmussen, O. Bang, Zeonex microstructured polymer optical fiber: Fabrication friendly fibers for high temperature and humidity insensitive Bragg grating sensing. Opt. Mater. Express **7**(1), 286–295 (2017a)

G. Woyessa, A. Fasano, C. Markos, H.K. Rasmussen, O. Bang, Low loss polycarbonate polymer optical fiber for high temperature FBG humidity sensing. IEEE Photon. Technol. Lett. **29**(7), 575–578 (2017b)

G. Woyessa, J.M. Pedersen, A. Fasano, K. Nielsen, C. Markos, H.K. Rasmussen, O. Bang, Zeonex-PMMA microstructured polymer optical FBGs for simultaneous humidity and temperature sensing. Opt. Lett. **42**(6), 1161–1164 (2017c)

Z. Xiong, G.D. Peng, B. Wu, P.L. Chu, Effects of the zeroth-order diffraction of a phase mask on Bragg gratings. J. Lightwave Technol. **17**(11), 2361–2365 (1999)

W. Yuan, L. Khan, D.J. Webb, K. Kalli, H.K. Rasmussen, A. Stefani, O. Bang, Humidity insensitive TOPAS polymer fiber Bragg grating sensor. Opt. Express **19**(20), 19731–19739 (2011)

W. Yuan, A. Stefani, O. Bang, Tunable polymer fiber Bragg grating (FBG) inscription: Fabrication of dual-FBG temperature compensated polymer optical fiber strain sensors. IEEE Photon. Technol. Lett. **24**(5), 401–403 (2012)